Chapter 2

New Constraints on the Late Cretaceous/Tertiary Plate Tectonic Evolution of the Caribbean

R. DIETMAR MÜLLER, JEAN-YVES ROYER, STEVEN C. CANDE, WALTER R. ROEST and S. MASCHENKOV

We review the plate tectonic evolution of the Caribbean area based on a revised model for the opening of the central North Atlantic and the South Atlantic, as well as based on an updated model of the motion of the Americas relative to the Atlantic–Indian hotspot reference frame. We focus on post-83 Ma reconstructions, for which we have combined a set of new magnetic anomaly data in the central North Atlantic between the Kane and Atlantis fracture zones with existing magnetic anomaly data in the central North and South Atlantic oceans and fracture zone identifications from a dense gravity grid from satellite altimetry to compute North America–South America plate motions and their uncertainties. Our results suggest that slow sinistral transtension/strike-slip between the two Americas at rates roughly between 3 and 5 mm/year lasted until chron 25 (55.9 Ma). Subsequently, our model results in northeast–southwest-oriented convergence until chron 18 (38.4 Ma) at rates ranging between 3.7 ± 1.3 and 6.5 ± 1.5 mm/year from 65°W to 85°W, respectively. This first convergent phase correlates with a Paleocene–Lower Eocene calc-alkaline magmatic stage in the West Indies, which is thought to be related to northward subduction of Caribbean crust during this time. Relatively slow convergence until chron 8 at rates from 1.2 ± 0.9 to 3.6 ± 2.1 mm/year from 65°W to 85°W, respectively, is followed by a drastic increase in convergence velocity. After chron 8 (25.8 Ma), probably at the Oligocene–Miocene boundary, this accelerated convergence resulted in 92 ± 22 km convergence from chron 8 to 6, 127 ± 25 km from chron 6 to 5, and 72 ± 17 km from chron 5 to the present measured at 85°W near the North Panama Deformed Belt at convergence rates averaging 9.6 ± 3.1 and 9.6 ± 2.1 mm/year from chron 8 to 6 and chron 6 to 5, respectively, slowing down to 5.2 ± 1.3 mm/year after chron 5. Neogene convergence measured at the eastern Muertos Trough, at 17.5°N, 65°W, is 41 ± 18 km from chron 8 to 6, 58 ± 25 km from chron 6 to 5, and 22 ± 17 km from chron 5 to present day, at rates between 4.4 ± 1.7 and 1.6 ± 1.0 mm/year. These well-resolved differential plate motions clearly show an east–west gradient in plate convergence in the Neogene, correlating well with geological observations. We suggest that the Early Miocene onset of underthrusting of the Caribbean oceanic crust below the South American borderland in the Colombian and Venezuelan basins, the onset of subduction in the Muertos Trough, and folding and thrust faulting at the Beata Ridge and the Bahamas, and the breakup of the main part of the Caribbean plate into the Venezuelan and Colombian plates, separated by the Beata Ridge acting as a compressional plate boundary (Mauffret and Leroy, Chapter 21) may all be related to the accelerated convergence between the two Americas.

The main differences with previous analyses are that (1) our model results in substantial variations in convergence rates between the two Americas after chron 25 (55.9 Ma), (2) we have computed uncertainties for our North America–South America plate flow lines, and (3) we show Tertiary Caribbean plate reconstructions in an Atlantic–Indian hotspot reference system. Our absolute plate motion model suggests that the Caribbean plate has been nearly stationary since chron 18 (38.4 Ma). The east–west gradient in convergence between the Americas in the Neogene has not resulted in substantial eastward motion of the Caribbean plate, but rather contributed to causing its breakup into the Colombian and Venezuelan plates along the Beata Ridge where east–west-oriented compressional stresses are taken up. Our model also suggests that the eastward escape of the Caribbean plate in a mantle reference frame ceased when seafloor spreading started in the Cayman Trough, if the current interpretation of magnetic anomalies in the Cayman Trough is not grossly in error. Our model suggests that the opening of the Cayman Trough was accomplished by westward motion of the North American plate relative to a stationary Caribbean plate in a mantle reference system. This implies that subsequent North America–Caribbean and South America–Caribbean tectonic processes were no longer dominated by Cocos–Caribbean and Nazca–Caribbean plate interactions, as the latter had ceased to drive the Caribbean plate eastwards. We conclude that the west-northwestward motion of South America relative to a trapped, stationary Caribbean plate caused oblique collision along the passive margin of eastern Venezuela in the Neogene.

Caribbean Basins. Sedimentary Basins of the World, 4 edited by P. Mann (Series Editor: K.J. Hsü), pp. 33–59.

INTRODUCTION

Many decades of research on deciphering the tectonic and sedimentary history of the Caribbean area (Fig. 1) have resulted in a fairly well understood tectonic framework of its evolution. The plate tectonic history between the two Americas has been reconstructed based on regional geophysical and geological data and its implications for Caribbean geology and have been evaluated in syntheses including Pindell et al. (1988), Ross and Scotese (1988), Pindell and Barrett (1990) and Stéphan et al. (1990). Our analysis builds on the knowledge that has accumulated from these and many other regional studies pertaining to Caribbean tectonic history. The purpose of this paper is not a comprehensive review of Caribbean tectonic evolution. Hence the reader will not find tables of syntheses of all tectonic events that may have occurred during Caribbean tectonic history, or all models that have been put forward to explain them. This information has been thoroughly reviewed by Pindell and Barrett (1990). Here we rather focus on extracting information from recently declassified dense satellite altimetry data that allow us to map the structure of the ocean floor in much more detail than previously possible and to

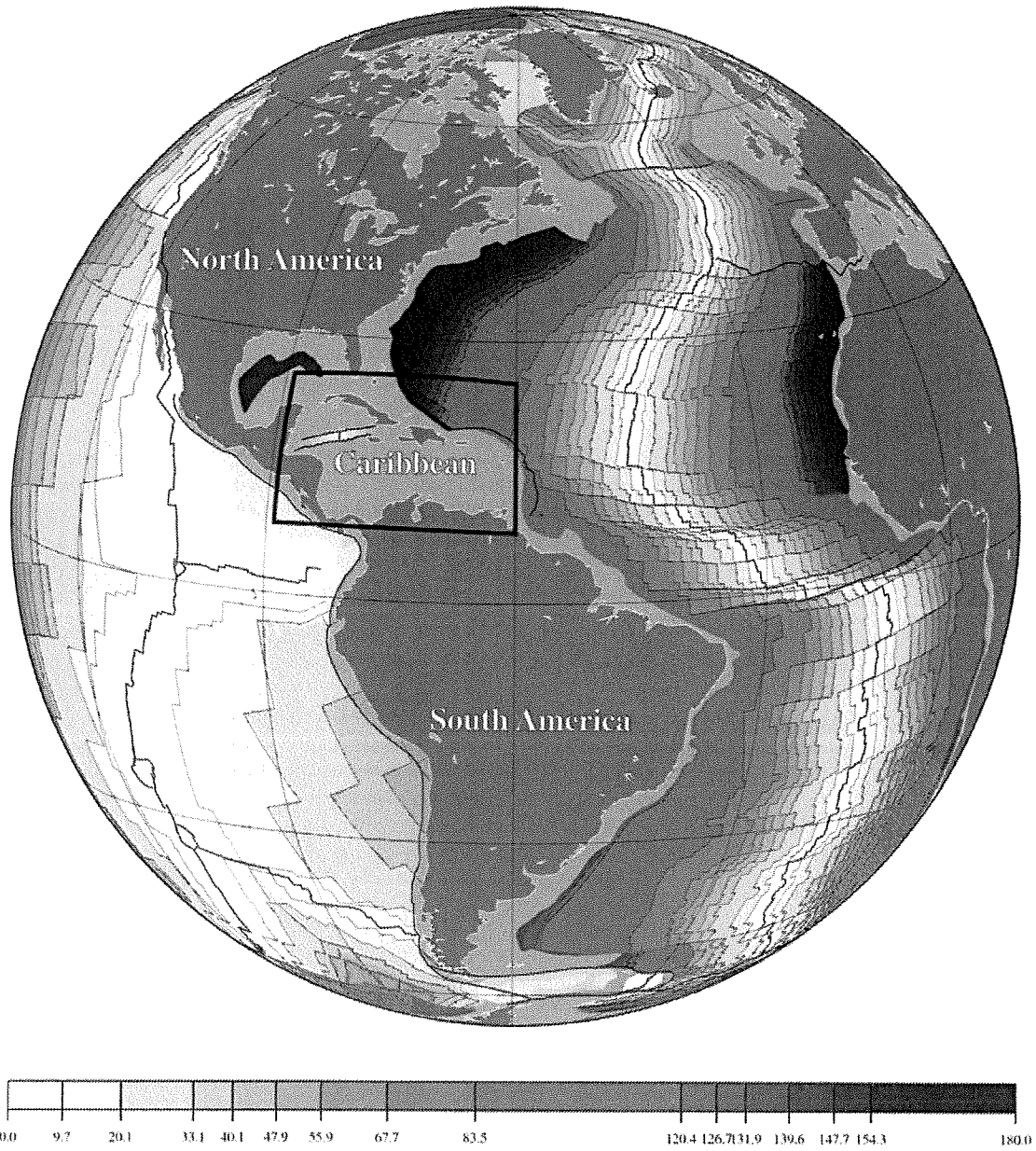

Fig. 1. Seafloor spreading isochrons in the Atlantic and eastern Pacific oceans from Müller et al. (1997). Light gray shades correspond to young ocean floor ages and dark grays to old ages. The bold frame outlines the Caribbean area shown in Fig. 2.

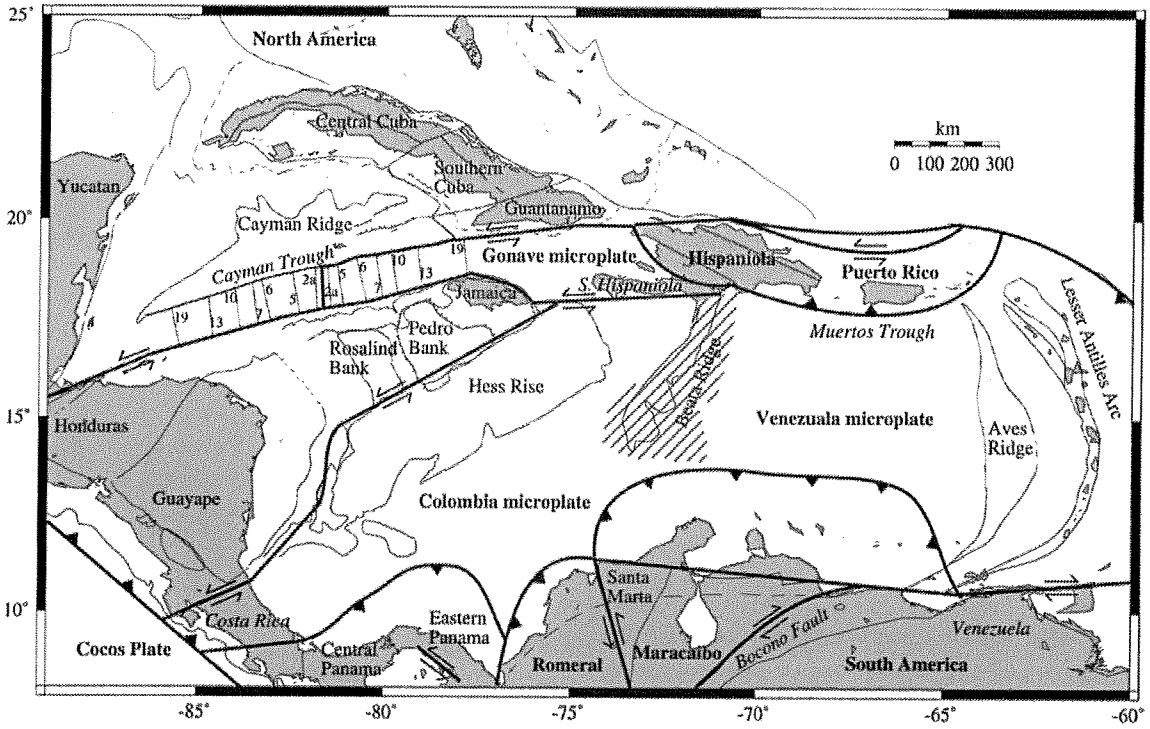

Fig. 2. Main tectonic elements of the Caribbean area. Isochrons shown in the Cayman Trough are from Rosencrantz et al. (1988). The cross-hatched area centered on the Beata Ridge indicates the plate boundary between the Venezuelan and Colombian microplates. Regional names which are not tectonic elements are shown in italics.

better constrain past plate motions along consuming or transform plate boundaries such as the boundaries between the North American, South American, and Caribbean plates (Fig. 2). We utilize these data jointly with new and existing magnetic anomaly data to investigate the Late Cretaceous and Tertiary plate kinematic framework of the Caribbean region, including the computation of uncertainties for our plate reconstructions.

Before the equatorial Atlantic between Africa and South America started opening at about chron M-0 time (120 Ma) (Pindell and Dewey, 1982; Mascle et al., 1988), the Caribbean tectonic framework was largely dependent on North America–Africa plate motions, which were identical to North America–South America motion vectors prior to the opening of the South Atlantic. After initial opening of the equatorial Atlantic, plate boundaries between the two Americas were affected by North America–South America relative plate motions resulting from the difference vectors between North America–Africa and South America–Africa seafloor spreading, as first computed by Ladd (1976). Reconstruction of the Caribbean tectonic frame for this period requires closure of the North America–Africa–South America plate circuit by using magnetic anomaly and fracture zone date sets that are standardized with respect to time. Because of the relatively slow velocity of North America–South America plate motions after chron 34 (83 Ma) it is particularly important to obtain estimates of the uncertainties for the relative plate motion vectors between the two Americas in order to evaluate the resolution of plate motions models.

We have combined a set of new magnetic anomaly data in the central North Atlantic between the Kane and Atlantis fracture zones, the 'Canary–Bahamas Transect' (Maschenkov and Pogrebitsky, 1992), with existing magnetic anomaly data in the central North and South Atlantic oceans as well as with Seasat and Geosat satellite altimetry data to create a self-consistent data set for the two ocean basins. The finite motion poles and their uncertainties were estimated for 15 times from chron 34 to the present using an inversion method developed by Chang (1987, 1988), Chang et al. (1990), and Royer and Chang (1991), which allows a simple parameterization of the rotation uncertainties along a plate circuit path. The resolution of the estimates for North America–South America plate motions differs through time and is largely dependent on the velocity of their relative motions, i.e. faster plate motions are better resolved than slower motions. Even though the first-order features of our model are similar to Pindell et al.'s (1988) model, our results differ in detail, especially in the late Tertiary, and we stress the evaluation of uncertainties of plate motion vectors. In particular, our conclusions differ from

Pindell et al. (1988) in that we suggest that North America–South America plate motions may have had substantial effects on the structural development of the Caribbean area after chron 34 (83 Ma), especially during a period of rapid plate convergence in the Neogene.

DATA

Magnetic anomaly data

The central North Atlantic is probably the ocean basin best covered by magnetic anomaly data. The three most comprehensive individual data sets are the northeast–southwest-trending Kroonvlag data (Collette et al., 1984), the trans-Atlantic Geotraverse (TAG) data set, which comprises a number of long east–west-oriented lines (Rona, 1980), and the Canary–Bahamas Transect (Maschenkov and Pogrebitsky, 1992), which comprises a dense set of survey lines between the Atlantis and Kane fracture zones from the Mid-Atlantic Ridge to about magnetic anomaly 13 (Fig. 3). These data sets are supplemented by a large number of other geophysical surveys (see Klitgord and Schouten, 1986, for previous compilation), resulting in dense data coverage.

A comprehensive analysis of magnetic anomaly data in the South Atlantic was carried out by Cande et al. (1988). In order to create a self-consistent set of magnetic anomaly identifications for closing the North America–Africa–South America circuit, we use Cande et al.'s (1988) magnetic anomaly crossings in the South Atlantic (Fig. 3) and identify the same magnetic chrons as Cande et al. (1988) in the central North Atlantic. All magnetic anomaly identifications correspond to the young end of normal-polarity intervals, except for anomaly 33o. The phase shift angles were determined from paleomagnetic poles for North America from Harrison and Lindh (1982) and from the IGRF90 reference field. We use the young end of the following normal-polarity intervals according to the Cande and Kent (1995) magnetic reversal time scale: chron 5 (9.74 Ma), 6 (19.05 Ma), 8 (25.82 Ma), 13 (33.06 Ma), 18 (38.43 Ma), 21 (46.26 Ma), 24 (52.36 Ma), 25 (55.90 Ma), 30 (65.58 Ma), and 32 (71.59 Ma), 33o (79.08 Ma), and 34 (83.00 Ma).

Fracture zone data

Fracture zones represent important information constraining plate motions and can be used in concert with magnetic anomaly data for computing

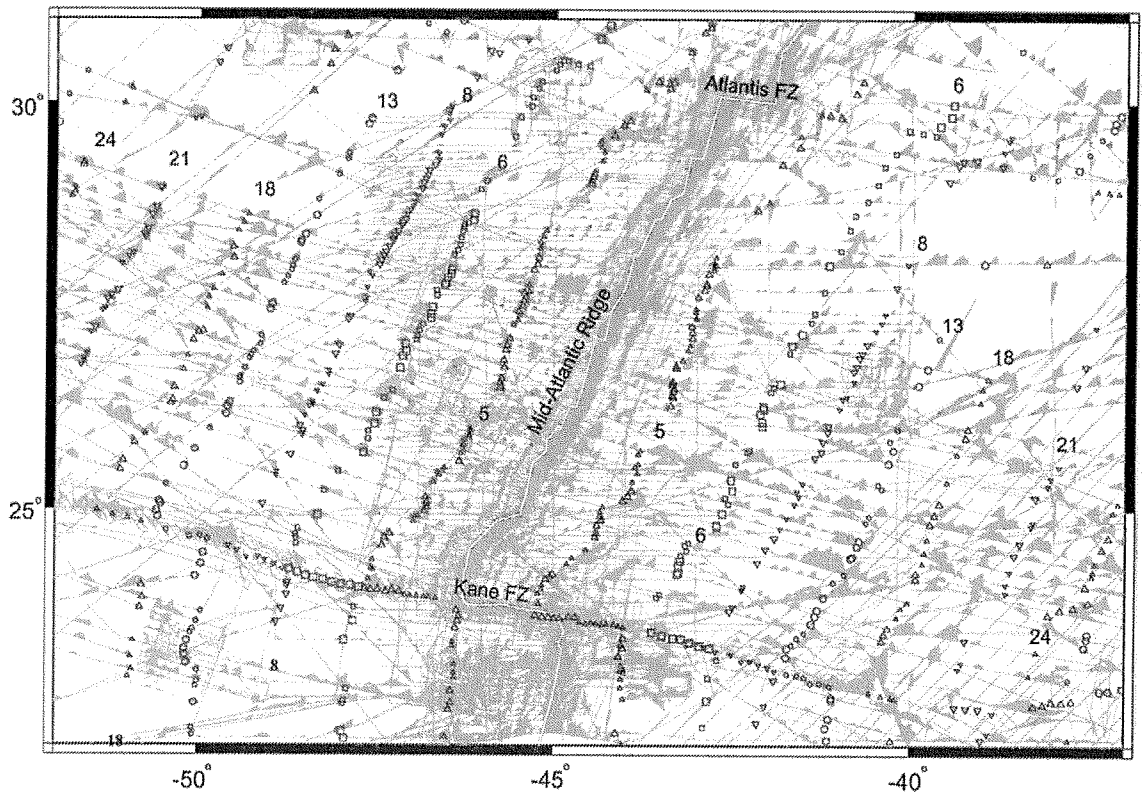

Fig. 3. New dense magnetic anomaly data in the Canary–Bahamas Transect area north of the Kane Fracture Zone (Maschenkov and Pogrebitsky, 1992), combined with data from other sources. Our magnetic anomaly identifications are shown as triangles (C5y, C18y, C24y), squares (C6y), upside-down triangles (C8y, C21y), and circles (C13y).

finite rotations. Geosat, Seasat and ERS-1 altimetry data provide a unique data set to uniformly map the height of the sea surface, whose short-wavelength topography reflects uncompensated basement topography, such as that related to fracture zones. Müller et al. (1991) demonstrated that there is an excellent correlation between the geoid anomaly and the basement structure of the Kane Fracture Zone in the central North Atlantic. They used geoid data from Geosat and subsatellite basement topography profiles of the Kane Fracture Zone to show that the average horizontal mismatch between geoid low and the axis of the basement trough, as mapped by Tucholke and Schouten (1988), is 5 km. The results of this comparative study represent 'ground truth' for the use of satellite altimetry data for accurately mapping slowly slipping Atlantic-type fracture zones.

Following the Kane Fracture Zone study, Müller and Roest (1992) identified a number of small- and medium-offset fracture zones from the along-track Geosat and Seasat gravity data by picking the center of the gravity troughs corresponding to the deepest portion of the central fracture valleys. We re-identified these fracture zones from dense satellite-derived gravity data (Sandwell and Smith, 1997). For the central North Atlantic reconstructions we use the Atlantis, Northern and Kane fracture zones (Fig. 4). When fracture zone offsets change from medium to small, as has happened in the case of the Northern Fracture Zone, whose offset diminished from 80 km at chron 25 to 20 km at chron 13, they may become unstable and commence to migrate along the ridge, producing V-shaped patterns. We used only those portions of fracture zones that appear to follow flow lines, i.e. have not migrated along the ridge axis. The location of the Kane Fracture Zone is constrained by Tucholke and Schouten's (1988) compilation of basement structure.

Numerous fracture zones from the equatorial Atlantic to the southern South Atlantic record plate flow lines of seafloor spreading in the South Atlantic. Shaw and Cande (1990) pointed out that the northernmost fracture zones in this spreading system, i.e. the Marathon, Mercurius, Doldrums, and Four-North fracture zones in the equatorial Atlantic (Fig. 2), put important constraints on South America–Africa plate motions due to their proximity to the finite rotation poles. However, because no

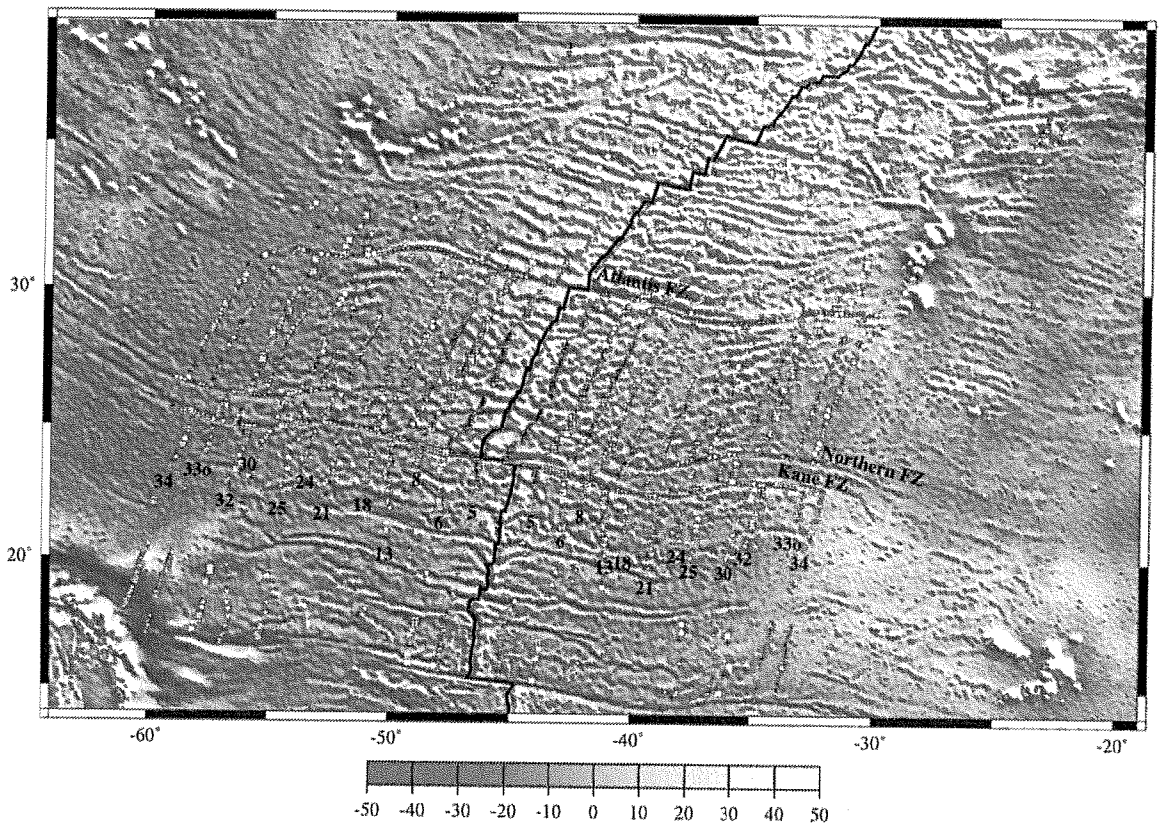

Fig. 4. Gravity anomalies from satellite altimetry from Sandwell and Smith (1997) and interpreted and rotated magnetic anomaly and fracture zone identifications in the central North Atlantic. The unrotated magnetic and fracture zone identifications are identified by the following symbols: triangle (C5, 9.74 Ma; C18, 38.43 Ma; C30, 65.58 Ma); square (C6, 19.05 Ma, C21; 46.26 Ma; C32, 71.59 Ma), upside down triangle (C8, 19.05 Ma; C24, 52.36 Ma; C33o, 79.08 Ma), circle (C13, 33.06 Ma; C25, 55.90 Ma; C34, 83 Ma). All rotated data points are marked by crosses. Paleoridge or transform segments as defined by magnetic anomaly or fracture zone identifications, approximated as great circles in the inversion method used here, are denoted by alternating small and large symbols.

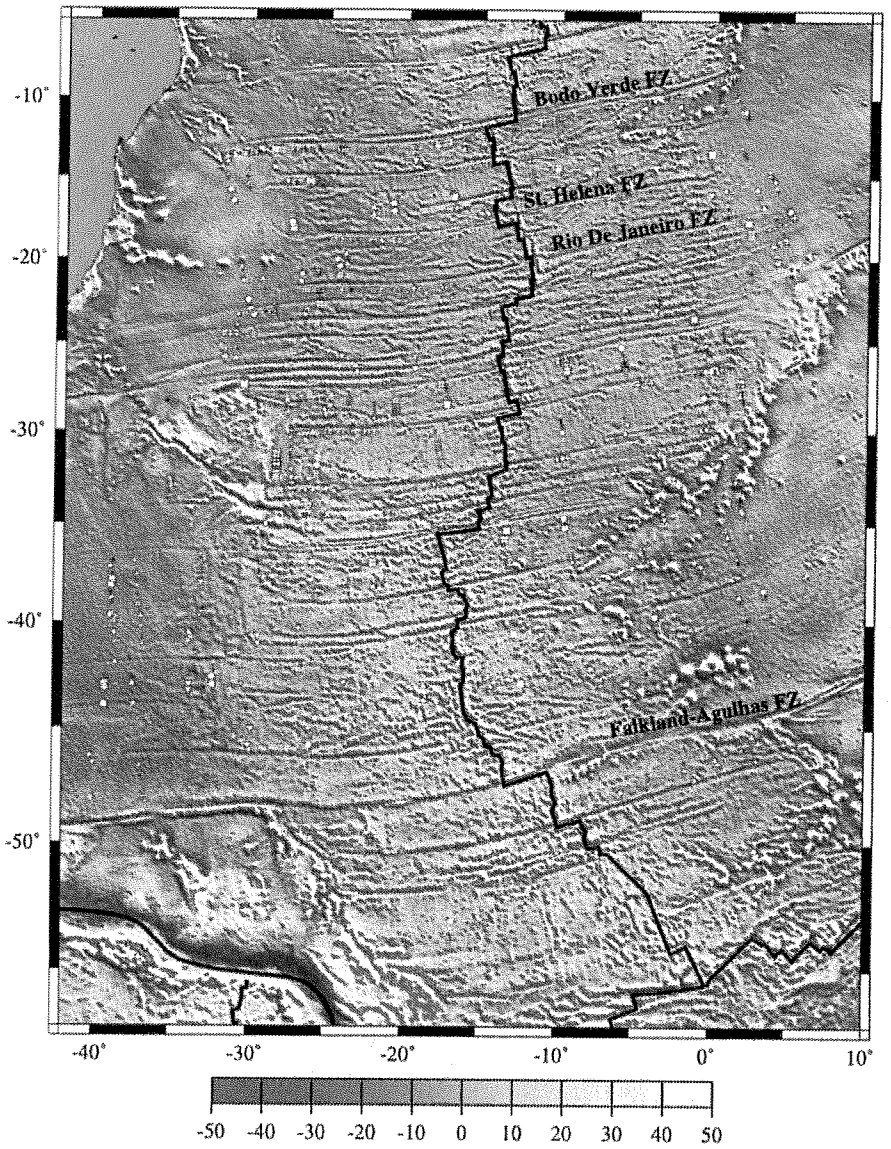

Fig. 5. Gravity anomalies from satellite altimetry from Sandwell and Smith (1997) and interpreted and rotated magnetic anomaly and fracture zone identifications in the South Atlantic. The symbols used for plotting magnetic and fracture zone identifications follow the same convention as in Fig. 4.

magnetic anomaly data have been identified in this area, we cannot resolve which portion of a fracture zone is relevant for a particular age, and whether these fracture zones reflect South America–Africa spreading for their entire length. We find that by using fracture zones south of 8°S only, we obtain very similar rotations compared with reconstructions in which equatorial fracture zones are included. Accordingly, our South Atlantic reconstructions are constrained by the Bodo Verde, Martin Vaz, Río Grande, and some unnamed fracture zones (Fig. 5). Both in the central North Atlantic and the South Atlantic only those fracture zones were used whose offsets through time are constrained by magnetic anomaly data. This is important, because the use of incorrect fracture zone segments for constraining a given reconstruction would skew our results. We also avoid large-offset fracture zones, as they are not reliable indicators of plate motion changes over short geological time spans.

RECONSTRUCTION METHOD

The finite plate motion poles and their uncertainties were estimated using an inversion method developed by Chang (1987, 1988), Chang et al. (1990), and Royer and Chang (1991), based on the criterion of fit by Hellinger (1981). The uncertainties of a rotation are expressed as a covariance matrix,

which is conceptually equivalent to the 'partial uncertainty rotations' described by Stock and Molnar (1983). In this method magnetic anomaly and fracture zone data are both regarded as points on two conjugate isochrons, which consist of great circle segments. The best fit reconstruction is computed by minimizing the sum of the misfits of conjugate sets of magnetic anomaly and fracture zone data points with respect to individual great circle segments. Consequently, both the resulting best-fitting rotations, as well as the sum of the misfits, depend critically on correctly identifying conjugate data points that belong to a common isochron segment. In practice, the application of Hellinger's criterion of fit poses no problem, because rotations have been published for most plates describing their Late Cretaceous/Tertiary history of motion. Hence, a starting rotation can be used for an initial reconstruction to identify conjugate isochron segments and data points.

A possible disadvantage of applying Hellinger's (1981) criterion of fit to both magnetic and fracture zone data is that fracture zones cannot necessarily be expected to fit as well as magnetic anomaly data. Although all portions of a fracture zone have at some time been the location of a transform fault and part of an isochron, fracture zone morphology becomes overprinted successively at the transform–ridge intersections during changes in spreading direction. The amplitude of this effect is expected to increase as a function of transform length. For this reason we do not use fracture zones with offsets of more than about 150 km. Shaw and Cande (1990) recognized this problem and suggested an inversion method that incorporates fracture zones by minimizing the misfit of fracture zone data with respect to plate flow lines. The benefits of this model were expected to be a utilization of the 'integral constraints' of fracture zones, i.e. their continuity, as well as the possibility of allowing for consistent asymmetries of fracture zone limbs on conjugate plate flanks. Shaw and Cande (1990) implemented this method by minimizing the misfits of fracture zone data to symmetric flow lines. However, forcing fracture zones to fit symmetric flow lines may obscure distinct changes in spreading direction recorded in fracture zones bounded by two asymmetrically spreading corridors. Even though seafloor spreading appears to be remarkably symmetric in the long run, accretion of ocean floor through time periods of short 'stages' resolvable by magnetic anomaly data can be quite asymmetric.

A critical aspect in our reconstruction method is the correct assessment of the uncertainties in the location of the data that will propagate into the uncertainties on the rotation parameters (location of the rotation pole and rotation angle). Following a detailed analysis of the dispersion of magnetic anomaly-5 crossings in the Indian Ocean by Royer et al. (1997) we assigned $1-\sigma$ nominal uncertainties of 4 km to the magnetic anomaly crossings and of 5 km to fracture zone crossings following Müller et al.'s (1991) analysis. The uncertainties assigned to the data ($\hat{\sigma}$) are related to their true unknown estimates (σ) by the quality factor:

$$\kappa = \left(\frac{\hat{\sigma}}{\sigma}\right)^2$$

Although κ is unknown, the method developed by Royer and Chang (1991) allows to estimate $\hat{\kappa}$ from the misfit, the geometry of the plate boundary and the number of data:

$$\hat{\kappa} = \frac{N - 2s - 3}{r}$$

where N is the number of points, s the number of great circle segments, and r the total weighted misfit. Note that $N - 2s - 3$ corresponds to the number of degrees of freedom.

Thus the parameter $\hat{\kappa}$ indicates whether the assigned uncertainties are correct ($\hat{\kappa} \approx 1$), underestimated ($\hat{\kappa} \ll 1$) or overestimated ($\hat{\kappa} \gg 1$). Our reconstructions indicate that our nominal uncertainties are generally slightly overestimated. For the central Atlantic, $\hat{\kappa}$ ranges from 1.07 to 3.08 and all degrees of freedom are larger than 50. This means that the average true uncertainties range from 2.3 ($= 4/\sqrt{3.08}$) to 3.9 ($= 4/\sqrt{1.07}$) km for the magnetic crossings, and 2.8 to 4.8 km for the fracture zone crossings (Table 1). For the South Atlantic, $\hat{\kappa}$ ranges from 0.67 to 1.74 with degrees of freedom between 28 and 42. Thus the uncertainties should lie between 3.0 and 4.9 km for the magnetic data, and 3.8 to 6.1 for the fracture zone data (Table 2). Several factors may contribute to this discrepancy in the dispersion of the magnetic crossings: (i) there are much less data in the South Atlantic, hence we are probably combining data from different spreading corridors into individual segments; (ii) there are much less recent (i.e. GPS-navigated) cruises in the South Atlantic than in the Central Atlantic. Without further investigating this question, we decided to keep an uncertainty of 4 km for the magnetic crossings. Our inversions also suggest that the dispersion of the fracture zone data is generally better than 5 km. However, since fracture zones are not the optimal records for plate reconstructions, and since we do not know how well gravity troughs relate to the actual location of (paleo-)transform segments, we choose to remain conservative and use the Müller et al. (1991) result of an uncertainty of 5 km for fracture zones.

Table 1

North America–Africa finite rotations

Chron	Age (Ma)	Latitude (+°N)	Longitude (+°E)	Angle (°)	r (km)	$\hat{\kappa}$ (km^{-1})	df	N	s	$\hat{\sigma}_{mag}$ (km)	$\hat{\sigma}_{fz}$ (km)
5	9.7	80.98	22.82	2.478	76.3	2.46	188	271	40	2.5	3.2
6	19.0	80.89	23.28	5.244	62.3	1.96	122	191	33	2.9	3.6
8	25.8	79.34	28.56	7.042	39.9	2.53	101	140	18	2.5	3.1
13	33.1	75.99	5.98	9.767	79.2	1.19	94	159	31	3.7	4.6
18	38.4	74.54	0.19	11.918	36.9	1.65	61	94	15	3.1	3.9
21	46.3	74.23	−5.01	15.106	42.9	1.19	51	96	21	3.7	4.6
24	52.4	77.34	−1.61	16.963	17.8	3.08	55	94	18	2.3	2.8
25	55.9	80.64	6.57	17.895	51.7	1.26	65	110	21	3.6	4.5
30	65.6	82.74	2.93	20.84	80.6	1.07	86	135	23	3.9	4.8
32	71.6	81.35	−8.32	22.753	66.9	1.33	89	142	25	3.5	4.3
33o	79.1	78.64	−18.16	26.981	55.2	1.85	102	155	25	2.9	3.7
34	83.0	76.81	−20.59	29.506	52.1	1.82	95	144	23	3	3.7

Parameters are: r = sum of misfits; N = number of data points; s = number of great circle segments; df = degrees of freedom; $\hat{\kappa} = \mathrm{df}/r$ (see text for discussion). The parameters $\hat{\kappa}$ and the misfit r in this table are calculated with nominal uncertainties of 4 km for the magnetic anomaly crossings and 5 km for the fracture zone crossings. The 'true' data uncertainties $\hat{\sigma}_{mag}$ and $\hat{\sigma}_{fz}$ are related to their unknown estimates (σ) (i.e. 4 and 5 km for magnetic and fracture zone data, respectively) by the quality factor $\kappa = (\hat{\sigma}/\sigma)^2$.

Table 2

South America–Africa finite rotations

Chron	Age (Ma)	Latitude (+°N)	Longitude (+°E)	Angle (°)	r (km)	$\hat{\kappa}$ (km^{-1})	df	N	s	$\hat{\sigma}_{mag}$ (km)	$\hat{\sigma}_{fz}$ (km)
5	9.7	62.05	−40.59	3.18	39.3	0.71	28	57	13	4.7	5.9
6	19.0	58.77	−37.32	7.049	26.3	1.10	29	58	13	3.8	4.8
8	25.8	57.59	−36.27	9.962	24.6	0.85	21	52	14	4.3	5.4
13	33.1	56.17	−33.64	13.41	52.4	0.67	35	64	13	4.9	6.1
18	38.4	57.10	−33.00	15.912	18.1	1.44	26	57	14	3.3	4.2
21	46.3	56.95	−31.15	19.107	47.1	0.89	42	79	17	4.2	5.3
24	52.4	58.89	−31.18	21.38	28.7	0.87	25	52	12	4.3	5.4
25	55.9	61.35	−32.21	22.273	27.7	1.01	28	53	11	4.0	5.0
30	65.6	63.88	−33.61	24.755	24.2	1.74	42	73	14	3.0	3.8
32	71.6	63.41	−33.38	26.573	24.1	1.16	28	53	11	3.7	4.6
33o	79.1	62.92	−34.36	30.992	20.7	1.74	36	65	13	3.0	3.8
34	83.0	61.88	−34.26	33.512	41.2	0.97	40	75	16	4.1	5.1

For explanation of parameters, see Table 1.

RESULTS

North America–Africa and South America–Africa finite rotations

Finite rotations for North America–Africa and South America–Africa plate motions were computed for 12 times from chron 34 to the present. The resulting finite rotations, statistical parameters, and covariance matrices are listed in Tables 1–4. The 95% confidence regions are 3-dimensional ellipsoids in latitude, longitude, and rotation angle space. In order to represent them on a map, the ellipsoids are projected onto the latitude–longitude sphere (cf. Royer and Chang, 1991). The projected uncertainty ellipses include uncertainties in both latitude, longitude, angle, but one must keep in mind that the true size of the rotation uncertainties (i.e. ellipsoids), which are described by the covariance matrices, might not be re-

Table 3

North America–Africa covariance matrices

Chron	a	b	c	d	e	f
5	4.721	−4.047	2.792	4.354	−2.897	2.064
6	6.134	−4.971	3.561	5.202	−3.586	2.679
8	17.122	−17.129	12.390	19.550	−14.054	10.432
13	8.318	−8.466	5.972	10.323	−7.144	5.207
18	19.815	−20.774	14.248	24.125	−16.397	11.551
21	18.001	−20.328	13.636	26.773	−17.973	12.551
24	26.464	−31.305	20.687	40.473	−26.665	17.992
25	11.855	−13.570	8.641	18.742	−11.775	7.871
30	9.118	−10.652	6.636	15.770	−9.831	6.448
32	12.322	−16.202	9.702	24.153	−14.573	9.103
33r	4.085	−4.022	2.339	5.730	−3.475	2.382
34	6.197	−4.831	2.468	6.957	−4.290	3.069

Covariance matrices can be reconstructed in the following way:

$$\begin{pmatrix} a & b & c \\ b & d & e \\ c & e & f \end{pmatrix} g$$

Table 4
South America–Africa covariance matrices

Chron	*a*	*b*	*c*	*d*	*e*	*f*
6	27.203	−7.073	−20.420	3.179	5.487	16.685
5	20.913	−4.353	−13.079	1.974	2.804	9.422
8	63.296	−20.659	−35.876	8.134	11.603	23.341
13	9.525	−2.385	−5.374	2.117	1.676	3.765
18	31.698	−12.098	−18.390	5.766	7.124	12.671
21	11.165	−3.955	−6.408	2.546	2.525	4.334
24	25.100	−11.021	−11.714	6.070	5.352	6.722
25	25.115	−11.568	−13.323	7.341	6.681	8.144
30	15.017	−6.988	−8.168	5.207	4.322	5.358
32	30.163	−13.978	−16.671	9.696	8.326	10.185
33r	9.249	−2.900	−4.696	3.493	2.513	3.347
34	8.711	−4.332	−4.971	4.014	3.230	3.649

For reconstruction of covariance matrices see Table 3.

flected well by their 2-D projection onto the sphere. For instance, in the case of the South Atlantic, the 2-D uncertainty in the location of the chron-5 best-fitting pole appears to be at least 10 times larger than the 2-D uncertainty in the location of the chron-21 rotation pole, whereas the volume of the 95% confidence region for chron-5 rotation is only about 3 times larger than for the chron-21 rotation (7838 versus 2773 km^3, respectively). Conversely, the 95% uncertainty volume for chron 8 (19,705 km^3) is 2.5 larger than for chron 5, whereas its 2-D projection is about 3 times smaller than for chron 5.

In Fig. 6 we compare our results with the North America–Africa pole path from Klitgord and Schouten (1986) and the South America–Africa pole path from Shaw and Cande (1990). The main difference for the central North Atlantic is that our path shows a sharp bend at anomaly-8 time (25.8 Ma), resulting in a pole path for chron 5 to chron 8 that is distinctly different from the chron-21 to chron-8 path, whereas Klitgord and Schouten's (1986) path is continuous between chrons 21 and 5. The consequences of this difference for Neogene North America–South American plate motions are discussed in subsequent sections.

Our South Atlantic pole path is generally similar to Shaw and Cande's (1990) path, but less smooth. The similarity reflects the fact that both models are based on very similar data sets, whereas the differences reflect properties of the different inversion methods used to compute finite rotations as well as new fracture zone identifications. The 'integral constraints' of fracture zone continuity used in Shaw and Cande's (1990) method is probably the main reason for the smoothness of their pole path. However, the use of symmetric flow lines to evaluate the fit of fracture zone data might smooth out real cusps in a finite pole path that is computed from reconstructing data from individual isochrons independently. The main difference between Shaw and Cande's (1990) model and our model for the South Atlantic (Fig. 5) is the anomaly-13 reconstruction, which results in a distinct cusp in our pole path, while there is a less accentuated cusp in their path. One way to qualitatively test whether or not such a cusp is supported by the data is to construct plate flow lines and evaluate their fit to fracture zones.

For South Atlantic spreading this is done best in the equatorial Atlantic, because the fracture zones here are the best recorders of changes in spreading direction due to their proximity to the finite motion poles. However, plotting plate flow lines in this area raises the problem of knowing where the South America–North American plate was located through time. Plotting flow lines both for North America–Africa and South America–Africa for the same fracture zone allows us to address this problem. We plot South Atlantic plate flow lines derived from our model in Fig. 7a with the gridded gravity anomaly field computed from Seasat, Geosat, and ERS-1 data (Sandwell and Smith, 1997). All flow lines are constructed using both ridge–transform intersections as seed points. The area encompassed by the resulting dual flow lines approximates the amount of transpression or transtension that occurred during changes in spreading direction, assuming symmetric plate accretion. The Marathon and Mercurius fracture zones do not fit the computed flow lines well. However, the Four-North and Doldrums fracture zones show a good fit to our flow lines. The latter observation confirms the validity of our South Atlantic plate motion model, whereas the former indicates that the North–South American plate boundary may be located in the vicinity of the Marathon and Mercurius fracture zones, resulting in deviations from South America–Africa flow lines. In comparison, we show central North Atlantic plate flow lines in the equatorial Atlantic Ocean in Fig. 7b. The Marathon Fracture Zone flow line clearly does not match the gravity anomaly expression of this fracture zone. The post-chron 6 flow line of the Mercurius Fracture Zone fits its eastern limb better than the South America–Africa flow line (compare with Fig. 7a), but not its western limb. Its is clear that this fracture zone would not be useful to constrain either North America–Africa nor South America–Africa plate motions, since it appears to have been affected by plate boundary processes. We can draw the conclusion that applying Hellinger's criterion of fit jointly to the magnetic anomaly data and fracture zone data from continuous fracture zones, which follow plate flow lines, and reconstructing these data independently for each isochron, results in plate models that produce smooth continuous flow lines, even though this property is not utilized or imposed by the model inversion, as it is in Shaw and Cande's (1990) method.

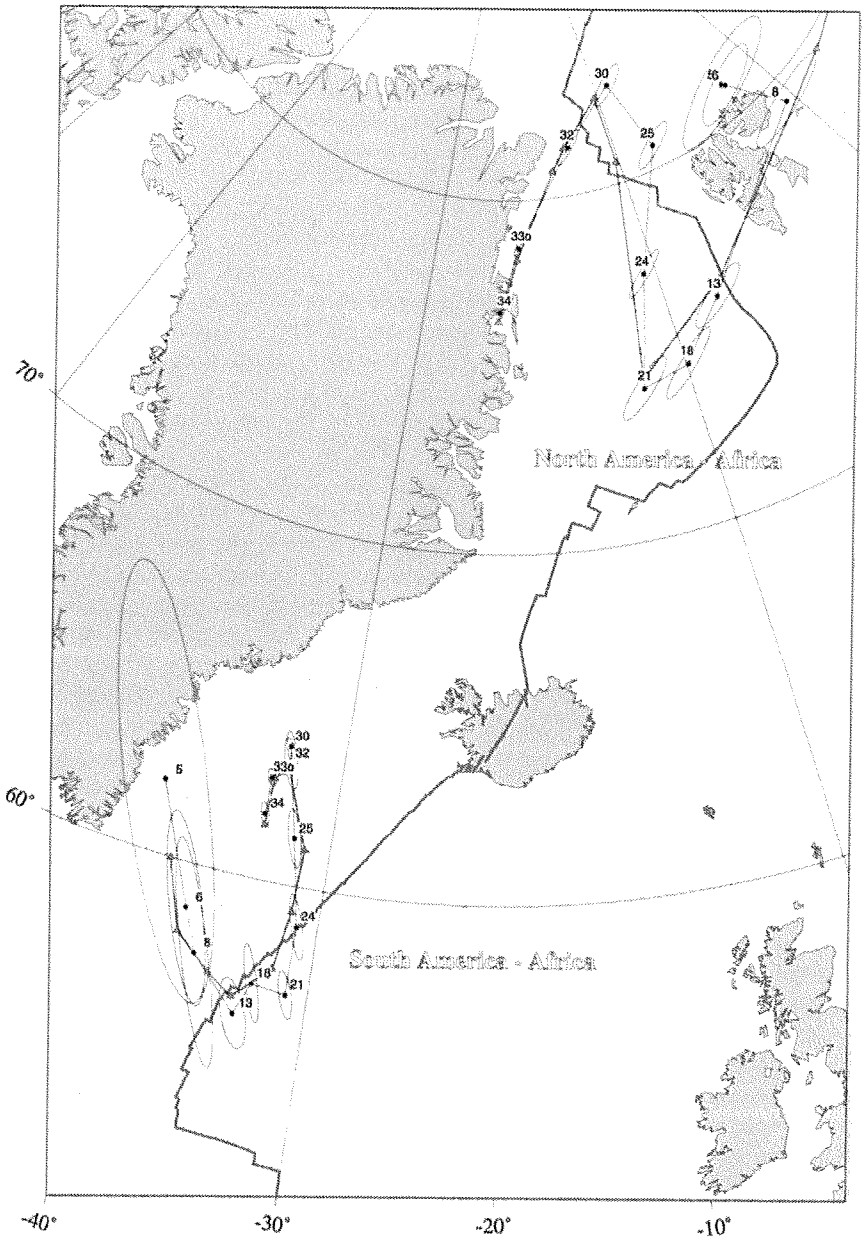

Fig. 6. Finite rotation poles and 95% confidence ellipses for North America–Africa (upper right) and South America–Africa (lower left) plate motions for 12 reconstruction times from chron 34 (83 Ma) to the present. As a comparison we show the North America–Africa pole path from Klitgord and Schouten (1986) and the South America–Africa pole path from Shaw and Cande (1990) (gray triangles). Note the sharp cusp in our North America–Africa pole path at chron 8 (25.8 Ma), resulting in a pole path for chron 5 to chron 8 that is distinctly different from Klitgord and Schouten's (1986) path. The differences between ours and both Klitgord and Schouten's (1986) and Shaw and Cande's (1990) models reflect a much improved accuracy in locating fracture zones based on a dense gravity anomaly grid from satellite altimetry (Sandwell and Smith, 1997), and some new magnetic anomaly data.

North America–South America finite rotations

Tables 5–8 list the rotation parameters for the North America–South America relative motions, for each chron resulting from the product of the South America–Africa rotation with the corresponding Africa–North America rotation (Table 9). The resulting pole path (Fig. 8) shows: (i) very stable poles of motion from chron 25 to 21, and from chron 18 to 8; (ii) an important northward migration of the rotation poles from chron 34 to chron 18; (iii) followed by a southward migration until chron 6. For this reason we computed only 8 stage rotations (Table 6) to describe the main episodes of relative motion between the two American plates. The North America–South America rotation stage poles always lie outside the Caribbean plate (Table 6); for the ages younger than chron 25 (55.9 Ma), they lie within or

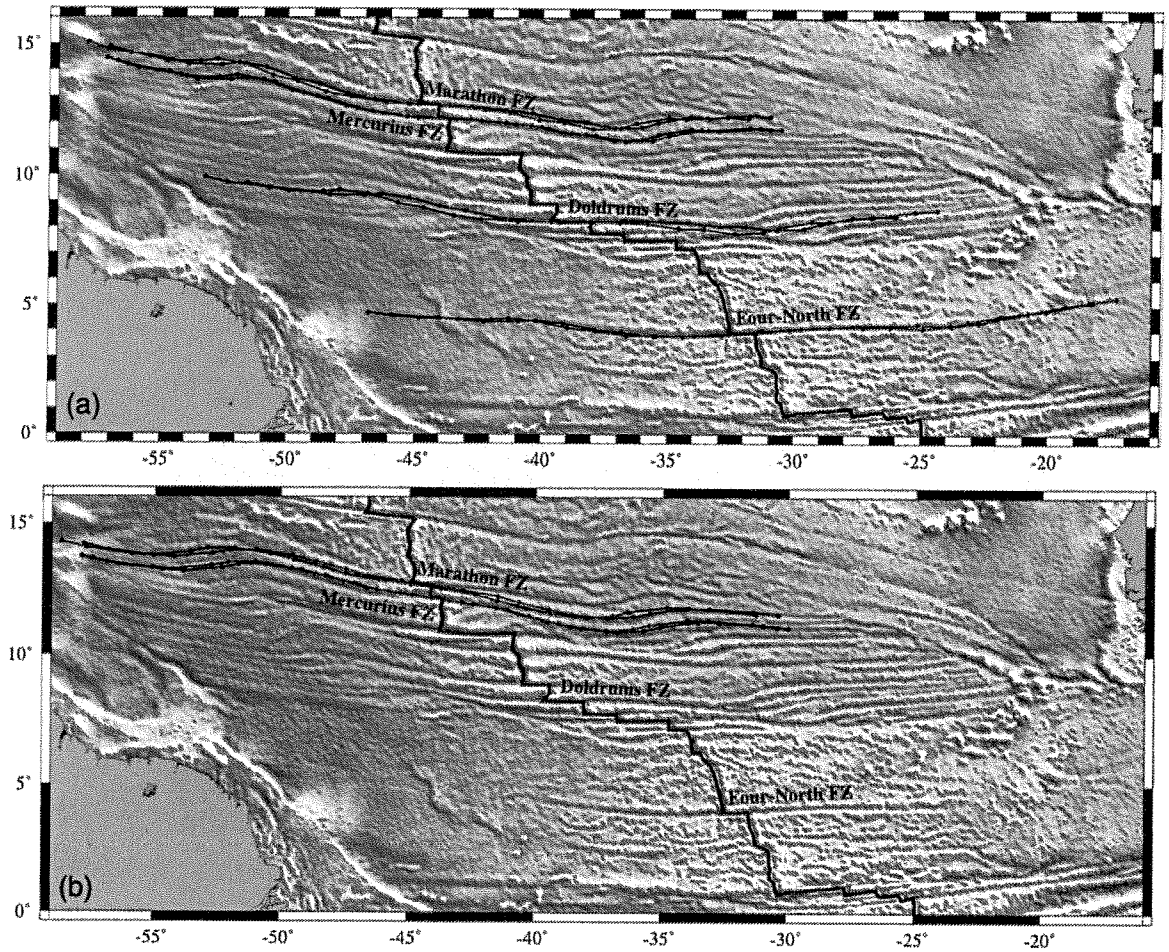

Fig. 7. (a) Gravity anomalies and South Atlantic symmetric plate flow lines in the Equatorial Atlantic Ocean. Flow lines are composed of segments for stages bounded by our reconstruction times (see Fig. 4). All flow lines have been constructed using both ridge–transform intersections as seed points. The area encompassed by the resulting dual flow lines approximates the amount of transpression or transtension that occurred during changes in spreading direction, assuming symmetric plate accretion. The Marathon and Mercurius fracture zones do not fit the computed flow lines well. However, the Four-North and Doldrums fracture zones show a good fit to our flow lines. The latter observation confirms the validity of our South Atlantic plate motion model, whereas the former indicates that the North–South American plate boundary may be located in the vicinity of the Marathon and Mercurius fracture zones, resulting in deviations from South America–Africa flow lines. (b) Gravity anomalies and central North Atlantic symmetric plate flow lines in the Equatorial Atlantic Ocean. The Marathon Fracture Zone flow line clearly does not match the gravity anomaly expression of this fracture zone. The post-chron-6 flow line of the Mercurius Fracture Zone fits its eastern limb better than the South America–Africa flow line (compare with Fig. 7a), but not its western limb. It is is clear that this fracture zone would not be useful to constrain either North America–Africa nor South America–Africa plate motions, since it appears to have been influenced by plate boundary processes.

in the vicinity of the North America–South America plate boundary, implying a different sense of motion along strike of this plate boundary.

North America–South America plate motions in the Caribbean area

Ideally we would like to be able to compute North America–Caribbean and South America–Caribbean plate motions and compare the modeled motion vectors with mapped plate boundary deformation. Accurate estimates for North America–Caribbean plate motions are available for times after chron 6 (19.0 Ma), as recorded by seafloor spreading in the Cayman Trough (Rosencrantz et al., 1988; Mauffret and Leroy, Chapter 21). The magnetic anomalies on older portions of the Cayman Trough are less straightforward to identify, and the chronology of both pre- and post-chron 6 seafloor spreading here is still the subject of debate. For these reasons we first analyze the North America–South America plate kinematic framework, as it is independent on knowledge of the spreading history in the Cayman Trough, and compare the results with geological and geophysical data from the northern and southern Caribbean plate boundaries.

Fig. 9 shows North America–South American plate motion through time, illustrated by the suc-

Table 5
North America–South America finite rotations

Chron	Age (Ma)	Latitude (+°N)	Longitude (+°E)	Angle (°)	df
5	9.7	15.06	−56.59	1.408	216
6	19.0	14.76	−52.43	3.433	151
8	25.8	17.52	−53.52	5.146	122
13	33.1	16.99	−53.13	6.067	129
18	38.4	18.12	−54.60	6.498	87
21	46.3	13.61	−53.09	7.11	93
24	52.4	13.95	−52.33	8.188	80
25	55.9	13.87	−53.04	8.777	93
30	65.6	11.25	−53.89	9.009	128
32	71.6	9.58	−53.74	8.947	117
33o	73.6	9.03	−56.57	9.12	138
34	83.0	7.31	−58.00	9.332	135

Table 6
North America–South America stage rotations (North America reference frame)

Stage (Chron a-b)	Age (Ma)	Latitude (+°N)	Longitude (+°E)	Angle (°)
0– 5	9.7	15.06	−56.59	1.408
5– 6	9.3	14.42	−49.56	2.03
6– 8	6.8	23.08	−55.54	1.727
8–18	12.6	20.57	−58.63	1.358
18–25	17.5	1.76	−49.85	2.355
25–30	9.7	−43.69	−80.57	0.484
30–33o	8.0	−31.75	−124.85	0.557
33o–34	9.4	−32.74	−102.67	0.417

cessive motion of three points attached to the North American plate with respect to the South American plate for eleven stages from chron 34 (83 Ma) to the present. The paths of these points through time as shown on Fig. 9 correspond to conventional plate flow lines illustrating relative North America–South America plate motion. The only difference here is that for each stage rotation vector a simultaneous 95% confidence region is plotted about the young ends of the relative motion vectors, i.e. the ellipse about points at chron 33o reflect the uncertainty for the chron 34–33o stage rotation. A simultaneous confidence region represents the area (on the surface of the Earth) in which a point on a given plate may have been located with equal likelihood for a particular reconstruction time, with 95% confidence. The simultaneous 95% confidence regions increase in size with increasing distance from the stage pole of motion; in the Caribbean area they increase in size correspondingly from east to west (Fig. 9).

The reader may note that even though the projected confidence ellipsoids of our finite rotation poles for North America–South American plate motion for chrons 18–6 show large overlaps (Fig. 8), the simultaneous 95% confidence regions for the three rotated points shown show only little overlap. This may appear puzzling, but only reflects the imperfect nature of the 3-dimensional finite rotation pole error ellipsoid projections onto a spherical surface on Fig. 8, as discussed before. In other words, this result shows that the covariance matrices and uncertainty ellipsoids for these reconstructions are different enough to distinguish different phases of convergence in the late Tertiary outside of the 95% error bounds.

We cannot resolve very slow relative motions between chrons 25 and 24; some overlap between the confidence regions for chrons 32 and 30 and chrons 18 and 13 is also observed. However, all other stage vectors are well resolved. Consequently, we compute a new set of 8 stage rotation poles (Table 6) and corresponding relative motion vectors, including only stages for which we can resolve relative North America–South America plate motions (Fig. 10). The relative motion vectors in this set of stages can be divided into four age groups: (1) slow sinistral strike-slip/transtension between chrons 34 and 25 ($\sim 2.8 \pm 0.8$–4.8 ± 1.1 mm/year at 85°W); (2) northeast–southwest-oriented conver-

Table 7
Covariance matrices for North America–South America finite rotations

Chron	*a*	*b*	*c*	*d*	*e*	*f*
5	25.693	−8.424	−10.306	6.305	−0.060	11.451
6	33.509	−12.099	−16.901	8.283	1.988	19.289
8	81.193	−38.062	−23.479	27.207	−2.057	33.476
13	18.284	−11.008	0.625	12.113	−5.265	8.859
18	52.534	−33.276	−4.194	29.357	−8.715	23.734
21	30.632	−24.772	7.601	27.959	−14.851	16.779
24	54.006	−43.018	9.682	44.281	−20.378	24.534
25	38.048	−25.517	−4.414	25.021	−4.705	16.000
30	25.161	−18.055	−1.233	19.886	−5.158	11.870
32	44.118	−30.783	−6.327	32.094	−5.741	19.408
33o	13.746	−7.130	−2.336	8.844	−0.753	5.696
34	15.362	−9.517	−2.616	10.472	−0.732	6.765

See parameter legend in Table 3.

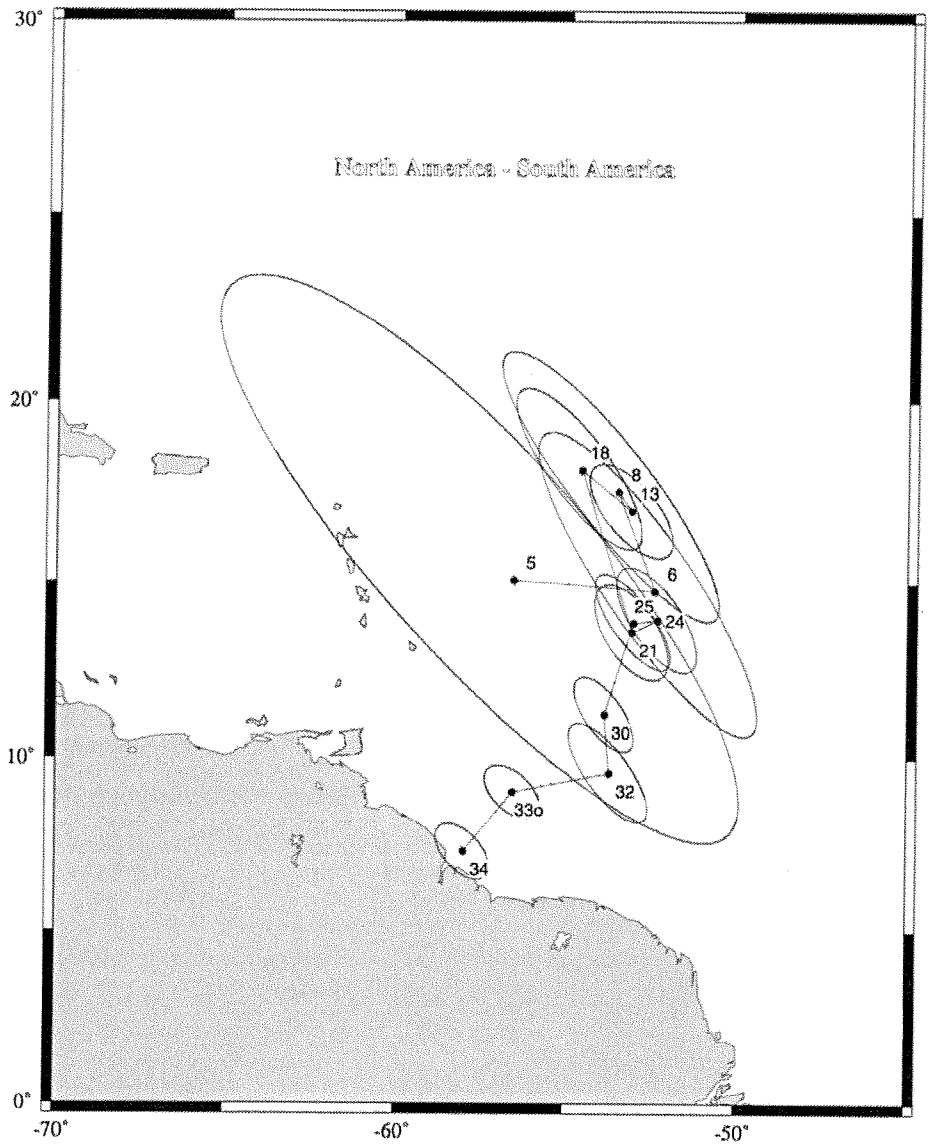

Fig. 8. Finite rotation poles for 12 reconstruction times for North America–South America relative plate motions since chron 34 (83 Ma). These poles have been computed by combining the finite rotations and their 95% confidence regions shown in Fig. 6. Note the large uncertainty for the chron-5 (9.7 Ma) reconstruction. This partly reflects that the South Atlantic reconstruction for this time is not well constrained. It also reflects that the uncertainty of finite rotations increases with decreasing finite rotation angle.

Table 8

Volumes of uncertainty ellipsoids for North–South America finite rotation poles

Chron	Latitude	Longitude	Angle	df	Vol. 95%	Vol. $1-\sigma$
5	15.06	−56.59	1.408	216	14,548	650
6	14.76	−52.43	3.433	151	22,448	993
8	17.52	−53.52	5.146	122	62,456	2741
13	16.99	−53.13	6.067	129	16,470	724
18	18.12	−54.6	6.498	87	46,085	1988
21	13.61	−53.09	7.11	93	28,396	1230
24	13.95	−52.33	8.188	80	48,212	2069
25	13.87	−53.04	8.777	93	38,850	1682
30	11.25	−53.89	9.009	128	26,246	1154
33o	9.03	−56.57	9.12	138	13,898	613
34	7.31	−58	9.332	135	14,696	647

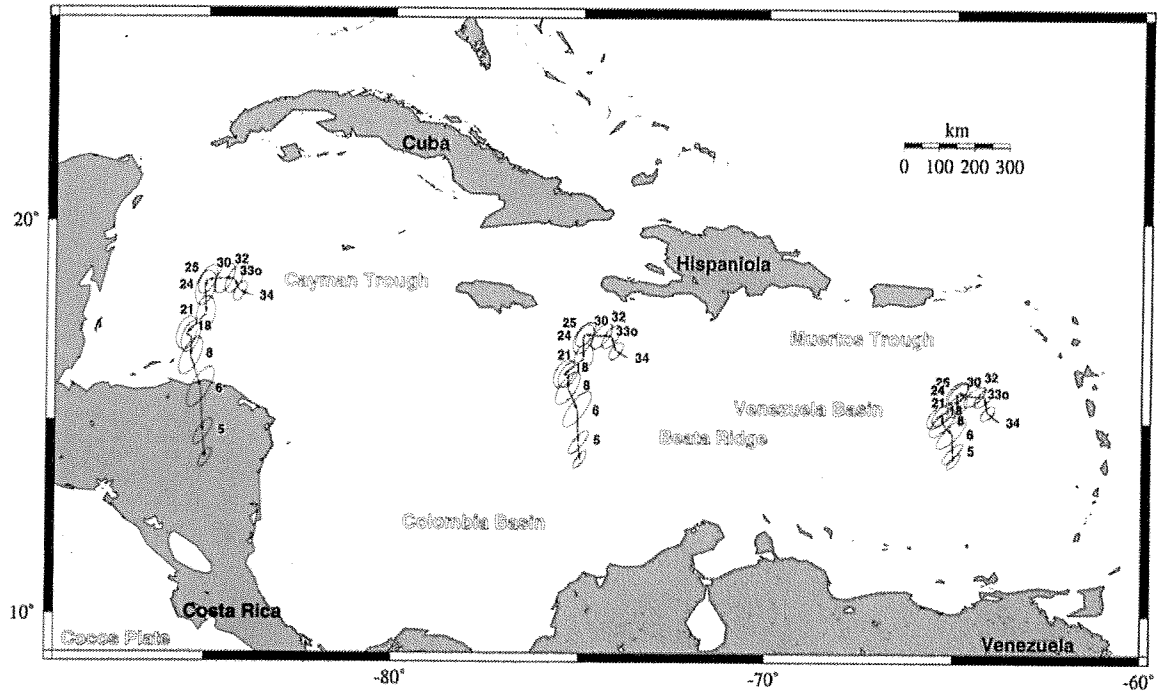

Fig. 9. North America–South America plate motion through time, illustrated by the successive motion of three points attached to the North American plate with respect to the South American plate for eleven stages from chron 34 (83 Ma) to the present. The paths of these points through time as shown on Fig. 9 correspond to conventional plate flow lines illustrating relative North America–South America plate motion. The only difference here is that for each stage rotation vector a simultaneous 95% confidence region is plotted about the young ends of the relative motion vectors, i.e. the ellipse about points at chron 33o reflect the uncertainty for the chron 34–33o stage rotation. A simultaneous confidence region represents the area (on the surface of the Earth) in which a point on a given plate may have been located with equal likelihood for a particular reconstruction time, with 95% confidence. This figure demonstrates that we cannot resolve very slow relative motions between chrons 25 and 24; some overlap between the confidence regions for chrons 32 and 30 and chrons 18 and 13 is also observed. However, all other stage vectors are well resolved. Consequently, we compute a new set of relative motion vectors, including only stages for which we can resolve relative North America–South America plate motions well, shown in Fig. 10.

gence from chron 25 to 18 (6.5 ± 1.5 mm/year at 85°W); (3) slow compressional motion from chron 18 to 8 (3.6 ± 2.1 mm/year at 85°W); and (4) fast north–south-oriented convergence from chron 8 to 6 (9.6 ± 3.1 mm/year for chrons 8–6 and 9.6 ± 2.1 mm/year for chrons 6–5 at 85°W), followed by a deceleration in north–south-oriented convergence post-chron 5 (5.2 ± 1.3 mm/year at 85°W).

In order to directly compare our model with Pindell et al.'s (1988) results, we compute North–South America relative motions for the same 7 stages as Pindell et al.'s (1988) (Fig. 11). The general shape of both models is similar, reflecting the similarity of the magnetic anomaly data sets used to constrain both models. The main difference between the models is that Pindell et al.'s (1988) model implies relatively constant convergence between the Americas of rates between 6 and 4 mm/year since chron 21 (46.3 Ma). Our model results in substantial variations in convergence rates since chron 25 (55.9 Ma), as documented in Fig. 10 and Table 10. In particular our model resolves the onset of fast convergence after chron 8 at a speed of nearly 10 mm/year, compared with less than 4 mm/year from chrons 18 to 8 measured at 85°W. Without identifying magnetic anomaly 8, two stages of slow (chron 13–8) and fast (chron 8–6) convergence would be averaged.

Table 9

Volumes of uncertainty ellipsoids for North America–Africa stage rotation poles

Stage	Latitude	Longitude	Angle	Vol. 95%	Vol. $1-\sigma$
5– 6	14.42	−49.56	2.03	36,317	1662
6– 8	23.08	−55.54	1.727	116,330	5324
8–18	20.57	−58.63	1.358	149,039	6821
18–25	1.76	−49.85	2.355	117,073	5358
25–30	−43.69	−80.57	0.484	87,663	4012
30–33o	−31.75	−124.85	0.557	56,368	2580
33o–34	−32.74	−102.67	0.417	39,294	1798

DISCUSSION

Lesser Antilles to Mid-Atlantic Ridge

The North America–South America plate boundary east of the Caribbean region is characterized by

Table 10
Uncertainties on motion vectors (3-D 95% confidence limits)

Chron	Time span (Ma)	Rate of motion (mm/year)	Motion vectors (km)	Azimuth (° from N)	r_{maj} (km)	r_{min} (km)	θ_{maj} (° from N)
Longitude: 48°W							
0– 5	9.7	1.6 ± 0.8	22 ± 10	−2	27	6	53
5– 6	9.3	0.6 ± 0.5	7 ± 7	−34	42	10	56
6– 8	6.8	3.6 ± 4.0	34 ± 38	48	55	12	57
8–18	12.6	1.6 ± 1.9	29 ± 33	30	54	12	58
18–25	17.5	2.4 ± 0.9	60 ± 23	−82	41	12	60
25–30	9.7	3.6 ± 1.0	49 ± 14	−64	34	11	62
30–33o	8.0	5.4 ± 0.7	61 ± 8	−33	27	11	60
33o–34	9.4	3.3 ± 0.6	43 ± 8	−42	24	12	60
Longitude: 52°W							
0– 5	9.7	0.7 ± 0.7	9 ± 10	−9	27	7	49
5– 6	9.3	1.0 ± 2.0	13 ± 25	−159	43	10	53
6– 8	6.8	2.7 ± 3.9	25 ± 37	72	56	13	53
8–18	12.6	1.0 ± 2.1	18 ± 38	44	55	15	54
18–25	17.5	2.6 ± 1.1	64 ± 28	−102	42	13	56
25–30	9.7	3.5 ± 1.1	48 ± 14	−67	35	12	58
30–33o	8.0	5.4 ± 0.8	61 ± 8	−35	28	12	57
33o–34	9.4	3.2 ± 0.6	42 ± 8	−45	24	12	56
Longitude: 58°W							
0– 5	9.7	0.3 ± 1.3	4 ± 18	−154	28	7	46
5– 6	9.3	2.4 ± 1.8	32 ± 23	−170	45	11	49
6– 8	6.8	2.6 ± 2.2	24 ± 21	108	58	15	49
8–18	12.6	0.7 ± 1.8	11 ± 33	84	57	17	50
18–25	17.5	3.0 ± 1.2	74 ± 30	−119	44	16	51
25–30	9.7	3.5 ± 1.1	48 ± 14	−71	36	13	54
30–33o	8.0	5.3 ± 0.8	61 ± 9	−37	28	13	52
33o–34	9.4	3.1 ± 0.6	42 ± 8	−48	25	12	52
Longitude: 65°W							
0– 5	9.7	1.6 ± 1.0	22 ± 13	172	29	8	41
5– 6	9.3	4.4 ± 1.7	58 ± 22	178	46	13	44
6– 8	6.8	4.2 ± 1.4	40 ± 13	136	60	19	44
8–18	12.6	1.2 ± 0.9	22 ± 15	138	59	22	43
18–25	17.5	3.7 ± 1.3	91 ± 32	−139	45	20	44
25–30	9.7	3.4 ± 1.1	47 ± 14	−76	38	16	46
30–33o	8.0	5.2 ± 0.9	59 ± 10	−39	30	14	45
33o–34	9.4	3.0 ± 0.7	40 ± 9	−52	26	13	45
Longitude: 75°W							
0– 5	9.7	3.5 ± 1.2	47 ± 16	174	30	10	35
5– 6	9.3	7.1 ± 1.9	94 ± 25	177	48	15	39
6– 8	6.8	6.8 ± 2.1	65 ± 20	154	63	22	37
8–18	12.6	2.4 ± 1.5	42 ± 26	161	64	26	34
18–25	17.5	5.1 ± 1.4	127 ± 34	−151	49	23	33
25–30	9.7	3.4 ± 1.1	47 ± 15	−85	41	19	35
30–33o	8.0	5.0 ± 1.0	57 ± 11	−45	32	16	35
33o–34	9.4	2.9 ± 0.7	38 ± 9	−60	29	14	36
Longitude: 85°W							
0– 5	9.7	5.2 ± 1.3	72 ± 18	174	31	11	30
5– 6	9.3	9.6 ± 2.1	127 ± 27	176	49	17	34
6– 8	6.8	9.6 ± 3.1	92 ± 30	161	66	25	31
8–18	12.6	3.6 ± 2.1	65 ± 36	167	68	29	27
18–25	17.5	6.5 ± 1.5	162 ± 38	−159	54	26	24
25–30	9.7	3.5 ± 1.1	47 ± 15	−93	45	21	26
30–33o	8.0	4.8 ± 1.1	55 ± 12	−51	35	17	26
33o–34	9.4	2.8 ± 0.8	37 ± 10	−70	31	15	28

The parameters r_{maj} and r_{min} are the semi-major and semi-minor axes of the ellipse of confidence (95% level). The variable θ_{maj} is the azimuth of the semi-major axis.

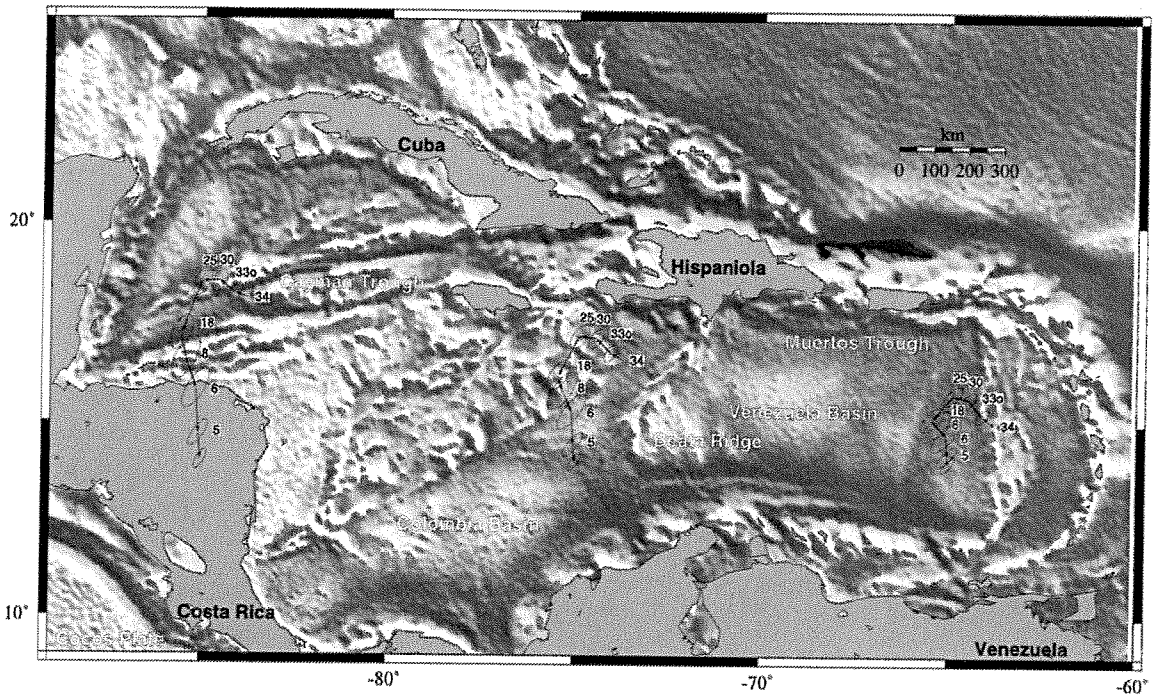

Fig. 10. Gravity anomalies in the Caribbean area and North America–South America plate motion through time of three points attached to the North American plate with respect to the South American plate for eight stages from chron 34 (83 Ma) to the present. The relative motion vectors can be divided into four groups: (1) slow sinistral strike-slip/transtension between chrons 34 and 25 (55.9 Ma) (~2.8 ± 0.8–4.8 ± 1.1 mm/year at 85°W); (2) northeast–southwest-oriented convergence from chron 25 to 18 (38.4 Ma) (6.5 ± 1.5 mm/year at 85°W; (3) slow motion from chron 18 to 8 (25.8 Ma) (3.6 ± 2.1 mm/year at 85°W); and (4) fast north–south-oriented convergence from chron 8 to 6 (19.0 Ma) (9.6 ± 3.1 mm/year for chrons 8–6 and 9.6 ± 2.1 mm/year for chrons 6–5 at 85°W), followed by a deceleration in north–south-oriented convergence post-chron 5 (9.7 Ma) (5.2 ± 1.3 mm/year at 85°W). See Table 6 for a complete list of stage motion vectors. Note acceleration in convergence at chron 8.

a number of anomalous ridges and troughs. The Barracuda and Tiburon ridges east of the Lesser Antilles Arc (Fig. 12) both exhibit unusually large Bouguer gravity anomalies (up to ~135 mGal). The eastern continuation of the plate boundary is expressed in the Researcher Ridge and Royal Trough (Fig. 12). The Royal Trough exhibits *en-échelon*-shaped tectonic fabric and fresh basalts on a basement characterized by spreading center type faulting identified from GLORIA data, whereas the Researcher Ridge has a large magnetic anomaly. Both features are interpreted as extensional structures (Collette et al., 1984; Roest and Collette, 1986).

For the area at the Tiburon and Barracuda ridges, our plate model results in a total of 151 ± 31 km left-lateral transtension from chron 34 (83 Ma) to 25 (55.9 Ma). A phase of slow transpression is predicted for chron 25 (55.9 Ma) to 18 (46.3 Ma), which is not well resolved, followed by extremely slow motion between chrons 18 and 6, during which time it is within the computed 95% confidence areas for the entire part of the plate boundary east of the Lesser Antilles subduction zone (Fig. 12). The plate boundary area east of 56°W was located quite close to the stage poles of motion; the resulting vectors of relative motion are so small that they cannot be resolved. Convergence in the Barracuda–Tiburon ridge area started at chron 6. We model 32 ± 23 km of convergence from chron 6 to 5, but virtually no relative motion after chron 5 (4 ± 18 km), which is much too small to be resolved, by our model. The post-chron 8 relative motion in the Royal Trough area can only be resolved for post-chron 5 time. Here our model implies 22 ± 10 km of extension for the last 10 million years.

Our plate model supports the suggestion that the present topographic and gravity expression of the Tiburon and Barracuda ridges may have resulted primarily from Neogene plate convergence (cf. Müller and Smith, 1993). In particular, the strong Moho uplift at the Tiburon Ridge, where the crust is modeled to be 1.5–2 km thick with a Moho uplifted more than 4 km (Müller and Smith, 1993), is extremely unstable. Without compressive forces, oceanic crust as thin as 1.5–2 km would subside and form a depression, rather than a ridge. The plate model used by Müller and Smith (1993) did not allow them to discriminate when in the Tertiary North–South America convergence in this area and the uplift of the two ridges might have been initiated. However, they argued that Middle Eocene–Late Oligocene turbidites on the slope of the Tiburon Ridge, which is now located 800 m above the abyssal plain, may

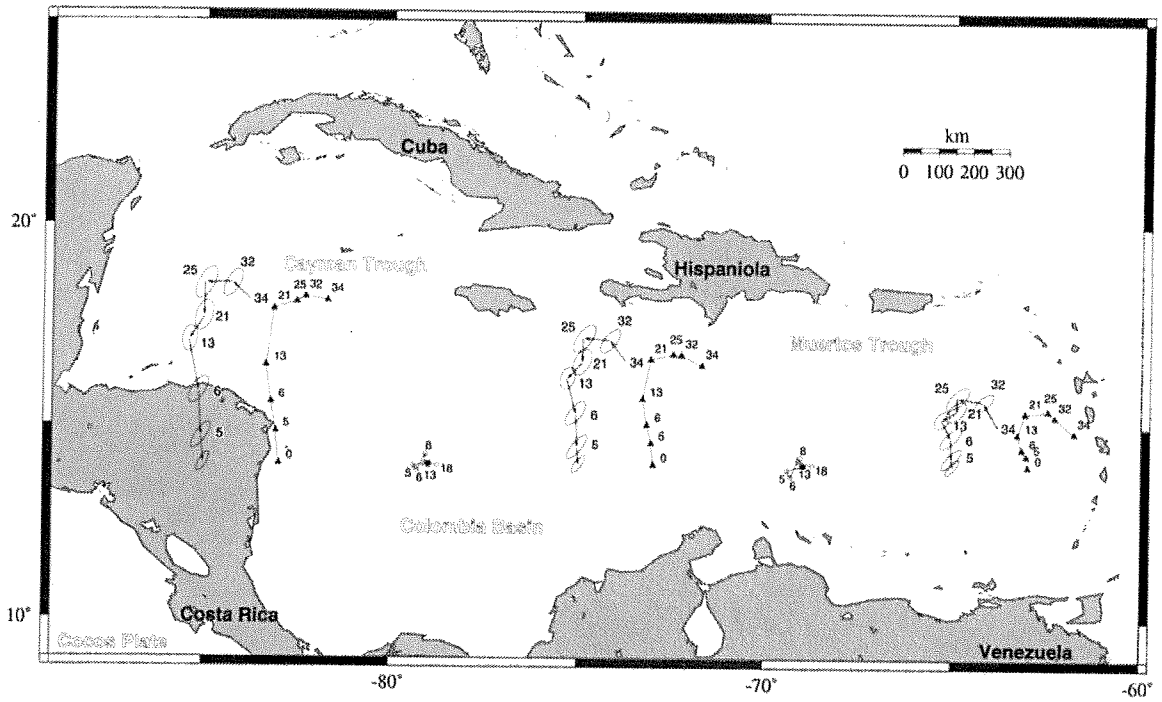

Fig. 11. North America–South America plate motion through time of three points attached to the North American plate with respect to the South American plate computed for the same seven stages as Pindell et al.'s (1988) model, shown by triangles. The general shape of both models is similar, reflecting the similarity of the magnetic anomaly data sets used to constrain both models. The main differences between the models are as follows. (1) Pindell et al.'s (1988) model implies sinistral strike-slip between North and South America from chron 34 to 21, followed by convergence. Our model implies strike-slip until chron 25, followed by convergence. (2) Pindell et al.'s (1988) model implies relative constant convergence between the Americas of rates of 4–6 mm/year since chron 21. Our model results in substantial variations in convergence rates from chron 25, as documented in Fig. 10 and Table 6. In particular we resolve the onset of fast convergence after chron 8 of nearly 10 mm/year, compared with less than 4 mm/year from chrons 18 to 8 measured at 85°W. This figure also shows the estimated motion of the Caribbean plate in a hotspot reference frame since chron 18 (38.4 Ma) (open circles); solid circles show the present-day position of the two points attached to the Caribbean plate used as starting points for these flow lines. See text for discussion.

indicate that most of its uplift occurred in post-Oligocene times, a conclusion strongly supported by the plate model presented here.

This idea contrasts the interpretation of Dolan et al. (1989, 1990), who suggested that the present topography of the Tiburon Ridge had existed prior to deposition of the turbidites, which would have been emplaced by upslope deposition from the abyssal plain onto the rise. Dolan et al. (1989, 1990) argue that the Tiburon Rise has existed as a bathymetrically shallow feature since the Late Cretaceous. An extensive discussion of this question can be found in Müller et al. (1993) and Müller and Smith (1993). We find that there is little evidence that would show conclusively that the present bathymetric elevation of the Tiburon Rise has existed since the Late Cretaceous. In contrast, the crustal structural modeling carried out by Müller and Smith (1993), together with the plate model presented here, indicates that much of the unusually shallow Moho topography and crustal uplift of the Tiburon Rise is a result of the onset of North America–South America convergence at chron 6 (19.0 Ma). A Neogene formation of the present topography of the Tiburon Rise would also alleviate the need for upslope turbidite deposition on the rise in the Middle Eocene–Late Oligocene, as suggested by Dolan et al. (1989, 1990). Instead, the present elevation of the turbidites on the slope of the rise would reflect post-depositional uplift.

Middle American Trench to Lesser Antilles

Our results suggest that slow sinistral transtension/strike-slip between the two Americas lasted from chron 34 (83 Ma) until chron 25 (55.9 Ma) (~2.8 ± 0.8–4.8 ± 1.1 mm/year at 85°W). However, we cannot attribute any particular Caribbean tectonic events to this phase of slow sinistral motion. Our model results in roughly northeast–southwest-oriented slow convergence from chron 25 (55.9 Ma) to chron 18 (38.4 Ma) (6.5 ± 1.5 mm/year at 85°W). This time period of convergence includes a calc-alkaline magmatic stage in the West Indies, dated as Paleocene–Lower Eocene (Perfit and Heezen, 1978), which is thought to be related to southward subduction of proto-Caribbean crust during this time. North–South America relative motion was characterized by relatively slow transpression

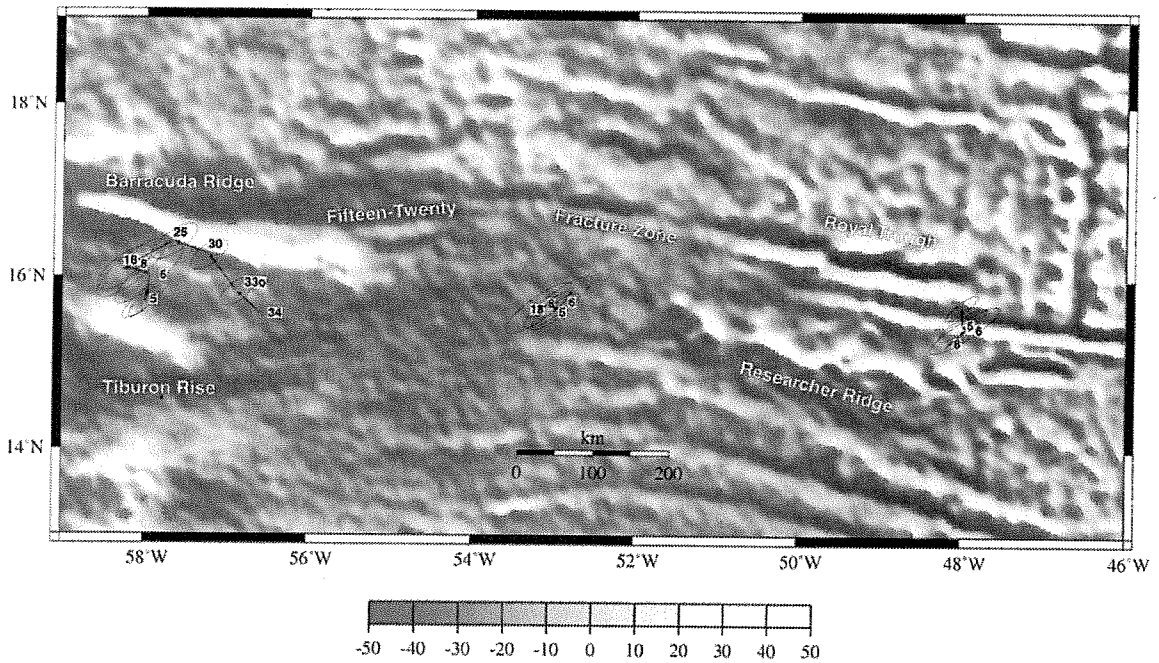

Fig. 12. North America–South America plate motion through time of three points attached to the North American plate with respect to the South American plate for eight stages from chron 34 (83 Ma) to the present and their simultaneous 95% confidence regions. Only the Barracuda Ridge area has been affected by North–South American plate motions as old as chron 34 (83 Ma). The ocean crust to the east becomes successively younger. The oldest relative motion vectors plotted correspond roughly to the age of the ocean crust south of the Fifteen-Twenty Fracture Zone. Relative plate motion in this area is not well resolved, except for oblique transtension in the Barracuda Ridge area from chron 34 to 25, and post-chron-6 north–south compression, post-chron-6 extension in the Royal Trough area. Color version at http://www.elsevier. nl/locate/caribas/

until chron 8 (25.8 Ma) (3.6 ± 2.1 mm/year at 85°W). This phase of slow relative motion between the two Americas correlates with a period of tectonic quiescence along some parts of the Caribbean margins during the Oligocene–Early Miocene that was characterized by subsiding basins, unconformably overlying the previously deformed belts (Calais et al., 1989). However, at the same time, collision has occurred off Venezuela (Mann et al., 1995).

Our model is different from Pindell et al.'s (1988) plate model for North–South America plate motions, in that it results in a drastic increase in convergence velocity subsequent to chron 8 (25.8 Ma) (9.6 ± 3.1 mm/year for chrons 8–6 and 9.6 ± 2.1 mm/year for chrons 6–5 at 85°W, compare also Figs. 10 and 11). A slowdown in convergence after chron 5 resulted in a post-chron-5 convergence rate drop to 5.2 ± 1.3 mm/year at 85°W. The modeled Neogene convergence results in 92 ± 30 km convergence from chron 8 to 6, 127 ± 27 km from chron 6 to 5, and 72 ± 17 km from chron 5 to the present near the North Panama Deformed Belt at 85°W (Fig. 10). The Neogene convergence measured south of the Muertos Trough at 65°W is 40 ± 13 km from chron 8 to 6, 58 ± 22 km from chron 6 to 5, and 22 ± 13 km from chron 5 to present day.

Geological data from the circum-Caribbean plate boundaries indicate that the tectonic regime changed drastically in the Early to Middle Miocene. The eastern portion of the North America–Caribbean plate boundary displays an accretionary wedge along the Muertos Trough (Case et al., 1984). Based on seismological evidence Byrne et al. (1985) showed that the Muertos Trough is an active structure and suggested it to be the site of subduction. North–south convergence is accommodated by oceanic crust underthrusting the Greater Antilles, or by folding and thrust faulting only, where the crust is thicker, as at the Beata Ridge and the Bahamas (Ladd et al., 1990). Correlation of seismic reflection data from the turbidite fill in the Muertos Trough with the Venezuelan Basin indicates a Neogene, or possibly late Neogene age for the initiation of underthrusting (Ladd et al., 1990). In the Early Miocene, the Peralta and Río Ocoa sediment groups on Hispaniola were deformed in a southwest verging fold-and-thrust belt (Heubeck et al., 1991), supporting evidence for the onset of Early Miocene convergence within this part of the Caribbean–North American plate boundary. Tectonic events at this time have also been mapped in the Dominican Republic, in Haiti, and on Cuba (Calais et al., 1992).

The Caribbean–South American plate boundary comprises a wide and complicated plate boundary zone. It starts at the deformation front of the subduction zone, includes various dextral strike-slip faults

of northern South America (e.g. Bocono, Oca, El Pilar) and continues to the south as a fold–thrust belt (e.g. Ladd et al., 1984). Biju-Duval et al. (1984) analyzed multichannel seismic reflection data in the Venezuelan Basin and concluded that the present configuration of the margin, i.e. underthrusting of the Caribbean oceanic crust below the South American borderland, developed in the Early or Middle Miocene. They also realized that north–south shortening observed at the North Venezuelan margin may be the result of regional North–South America convergence. Recently, a comprehensive analysis of new and existing seismic data from the Beata Ridge and adjacent areas by Mauffret and Leroy (Chapter 21) has shown that the Beata Ridge, a Cretaceous plateau, is bounded to the east by compressive structures reactivated by right-lateral strike-slip, and by normal faults to the west. Uplift of the ridge increases from south to north, and is estimated to have started in the Early Miocene (23 Ma), resulting in a total shortening between 170 km and 240 km as a function of latitude (Mauffret and Leroy, Chapter 21). They interpret the Beata Ridge as a compressional plate boundary, resulting from overthrusting of the Colombian microplate onto the Venezuelan microplate. The implied clockwise rotation of the Colombian microplate and convergence between the latter and the Venezuelan microplate are consistent with differential convergence between the North and South American plates, increasing from east to west, thereby 'squeezing' the Colombian plate out to the east, as suggested by Burke et al. (1978). Mauffret and Leroy (Chapter 21) suggest that the observed deformation may also be caused by the buoyancy of the Cocos plate, which is subducting under the Caribbean plate (England and Wortel, 1980; Meijer, 1992). However, Central America experiences extension in the back arc in the north where the subducting Cocos plate is older than in the south, whereas a younger Cocos plate in the south causes shortening. Alternatively, compression in Costa Rica, as expressed by the April 22, 1991 Costa Rica earthquake (Plafker and Ward, 1992), has been attributed to the subduction of an aseismic ridge (Adamek et al., 1987). Mann and Burke (1984) suggested that the Beata Ridge may be the consequence of northward motion of the Maracaibo block, a tectonic block of South America. Recent work has confirmed a north- to northeast-directed motion of these blocks relative to the Caribbean plate (Ego et al., 1995). In summary it is unclear what the role of the Cocos plate may be in terms of contributing to compression at the Beata Ridge.

An east–west gradient in convergence between the Americas is also supported by a recent analysis of present-day relative plate motions between North and South America based on GPS data (Dixon and Mao, 1997). They found an increase of differential north–south convergence from east to west from about 1 mm/year at the Barracuda ridge to about 9 mm/year at 85°E. It is interesting to note that their modeled present-day convergence rate of 9 mm/year at 85°E is similar to the rates we calculate for chron 8–5 time, and significantly faster than our post-chron-5 convergence estimate at 85°W of 5.2 ± 1.3 mm/year. It is not clear whether this difference reflects a recent acceleration in North America–South America plate convergence, or whether it is related to problems in our anomaly-5 reconstruction. The latter may well be the case, since the South Atlantic reconstruction for this time is not well constrained; it is based on a small number of data points only, and Table 2 shows that we have slightly underestimated the uncertainties of both magnetic and fracture zone identifications for this data set. In contrast, the anomaly-5 reconstruction in the central North Atlantic is extremely well constrained.

We propose that the post-chron-8 convergence between North and South America has also played a substantial role in the Neogene Panama Arc collision and subsequent arc deformation to an S-shaped pattern. In the collision area, the computed north–south convergence between the Americas resulted in a total of 291 ± 75 km of north–south convergence. During the Middle to Late Miocene the onset of the collision of the Costa Rica–Panama Arc with the western Cordillera of northwestern South America (Wadge and Burke, 1983; Eva et al., 1989; Mann et al., 1990) started forming the North Panama Deformed Belt.

The tectonic events outlined above are all slightly younger (mostly Early Miocene) than the onset of North–South America convergence predicted by our model (~26 Ma, Late Oligocene). This may reflect an artifact of our model. Our plate model lacks resolution between anomalies 8 (25.8 Ma) and 6 (19.0 Ma), because it is not straightforward to identify the magnetic anomalies between 6 and 8 with confidence in a slowly spreading tectonic regime. It is possible that the Early Miocene tectonic events in the Caribbean correspond to a global change in plate motions. Evidence for this idea comes from a detailed survey of the Pitman Fracture Zone in the South Pacific that shows a distinct change in spreading direction at chron 6c (Cande et al., 1995) which represents the Oligocene–Miocene boundary (23.8 Ma). It is virtually impossible to identify this magnetic anomaly in the slowly spreading central North Atlantic and South Atlantic oceans. Therefore, we consider it possible that convergence started at the Oligocene–Miocene boundary, 2 m.y. later than predicted by our plate model. Pindell et al.'s (1988) model results in an acceleration in convergence at chron 6 (20 Ma in the DNAG timescale

(Kent and Gradstein, 1986), 19 Ma in the timescale used here (Cande and Kent, 1995), with extremely slow convergence from chron 13 to chron 6. This demonstrates that a model not constrained by any magnetic anomaly identification between anomaly 6 and 13 (a time interval 14 m.y. long) results in an apparent acceleration in convergence at 19 Ma, about 5 m.y. later than the Oligocene–Miocene boundary.

Plate motions relative to the mantle

We put Caribbean plate motions into an absolute hotspot reference frame based on Atlantic–Indian ocean hotspot tracks (Müller et al., 1993) for understanding cause and effects of plate motions between the Americas and the Caribbean plate(s). Ross and Scotese (1988) used a paleomagnetic reference frame for their model (which cannot resolve longitudinal motions of plates), and correspondingly do not show a geographic frame on their reconstructions. Pindell et al. (1988) used the absolute plate motion model by Engebretson (1982) and Engebretson et al. (1985) for the Pacific based on hotspot tracks to calculate Pacific–Caribbean relative motions, which have likely exerted controls on Caribbean tectonic evolution in the Mesozoic and early Tertiary (Pindell et al., 1988), but not necessarily in the Neogene. In any case, Pacific absolute plate motions are only of limited use to constrain absolute motions of plates bordering the Atlantic Ocean, as our knowledge on closing plate circuits crossing the boundary between East and West Antarctica is still inadequate (Molnar and Stock, 1987; Cande et al., 1995).

We use the relative plate motion model for the central North Atlantic and South Atlantic presented here, a revised relative plate motion model for the Caribbean area, largely based on the tectonic elements and plate hierarchy from Ross and Scotese (1988), and the model for motion of plates in the Atlantic and Indian Ocean Hemisphere relative to major hotspots (Müller et al., 1993). The combined rotation model has been adapted to the Cande and Kent (1995) timescale for post-chron-34 (83 Ma) times and the Gradstein et al. (1994) timescale for earlier times.

The absolute plate motion model by Müller et al. (1993) is based on jointly fitting dated hotspot tracks on the Australian, Indian, African, and North and South American plates relative to present-day hotspots assumed fixed in the mantle. Therefore this model is better constrained than a model solely based on the hotspot tracks of one plate.

Pindell et al. (1988) suggested that most of the total opening by seafloor spreading between the two Americas was accomplished some time between 100 and 90 Ma, when the Caribbean plate started entering from the west. However, the age of the initial contact of a Caribbean plate originating from the Pacific has been revised to late Campanian–Maastrichtian, when syn-orogenic sedimentation and northward verging folding, thrusting and obduction of ophiolites have occurred at the southern margin of the Yucatán Peninsula in Guatemala (Rosenfeld, 1990). The arguments in favor of an allochthonous nature of the Caribbean oceanic crust have been reviewed comprehensively by Pindell and Barrett (1990).

In the Paleocene the Yucatán Basin opened along a left-lateral strike-slip fault (Rosencrantz, 1990) and the prograding arc started colliding with the Bahamas Platform in western Cuba (Bralower et al., 1993). For the time after the Middle Eocene we have an estimate for North America–Caribbean plate motions from the spreading history in the Cayman Trough (Rosencrantz et al., 1988), even though spreading here may not reflect the total North America–Caribbean motion (Rosencrantz and Mann, 1991). Burke et al. (1980) suggested that cumulative offsets of strike-slip faults on Jamaica suggest a minimum rate of offset of 4 mm/year, in addition to an average of 16 mm/year of total opening in the Cayman Trough. We implemented this suggestion in our rotation model, similar to Ross and Scotese (1988), by allowing for 4–6 mm/year of left-lateral strike-slip between Jamaica and southern Hispaniola. In Fig. 11 we show the resulting path of two points attached to the Caribbean plate relative to the mantle (without considering relative motion between the Colombian and Venezuelan microplates through time, which we cannot reconstruct). The two absolute plate motion paths in Fig. 11 as well as the plate reconstructions in Fig. 13b–d show that the Caribbean plate has been virtually stationary with respect to the mantle at least since the onset of seafloor spreading in the Cayman Trough. The errors from combining the 'absolute' and relative plate motions models involved in this calculation are probably larger than the total length of the path shown. The Caribbean plate could have only maintained a substantial eastward component of motion if either the Cayman Trough opened much later and faster than presently assumed, and/or if there has been much faster strike-slip between the Caribbean plate and Jamaica than suggested by Burke et al. (1980).

North America's and South America's plate motions in the mantle reference frame are both characterized by relatively fast westward motion, with a small component of convergence added at chron 13 due to a clockwise change in South American plate motion, and even faster convergence after chron 8 due to a counterclockwise change in North America absolute plate motions. In contrast, the Caribbean plate appears to have been virtually stationary in a mantle reference frame at least since chron 18. This

result agrees with an idea put forward by Sykes et al. (1982), who noted that only a small fraction of its perimeter is attached to a subducting slab. Even though the Caribbean slab under the South American plate has been shown to be longer than previously thought, the forces assumed to be most important for driving plates, namely ridge push, slab pull and trench suction (this force acts to draw plates together at a trench; Elsasser, 1971) must be relatively small. If they were not, then the Caribbean plate would not rest in a mantle reference frame, as found by our plate kinematic analysis.

Our result is also in accordance with the analysis by Gripp and Gordon (1990) of present-day Caribbean plate motions with respect to the hotspots. Their analysis, based on motion of the Pacific plate relative to its underlying hotspots, and the NUVEL-1 relative motion model by DeMets et al. (1990) results in roughly west-southwest-oriented motion of the Caribbean plate. However, their motion vectors do not differ significantly from zero.

It must be concluded that tectonic plate boundary processes between the Caribbean plate and the Americas are entirely driven by relatively fast, mostly westward motion of North and South America. The resulting differential motion between North and South America affects a stationary Caribbean plate trapped between two larger plates by edge-driven plate tectonic interactions, equivalent to some small plates in the Middle East (e.g. Arabia/Anatolian plate; McKenzie, 1972).

Sykes et al. (1982) recognized this possibility, but suggested alternatively that the Caribbean plate may be forced to move eastward in response to the gradient in convergence rate between North and South America, increasing from east to west, as also found by our analysis. In contrast, the plate motion paths plotted in Fig. 11 suggest that the eastward motion of the Caribbean plate with respect to the two Americas is entirely due to westward motion of the latter two plates with respect to the mantle, and that the east–west convergence gradient quoted by Sykes et al. (1982), which has been constrained to post-chron-8 (25.8 Ma) times by our model (probably post-chron 6c as discussed above), may not have resulted in substantial eastward motion of the Caribbean plate with respect to the mantle. Rather, the east–west gradient in post-chron-6c convergence may have contributed to causing east–west compression at the Beata Ridge, as described in Mauffret and Leroy (Chapter 21).

Our combination of relative and absolute plate motions indicates that throughout the Tertiary tectonic processes at the northern and southern boundary of the Caribbean plate were governed by the relatively fast westward motion of both the North and South American plates with respect to a nearly stationary Caribbean plate. The differences between North America–Africa and South America–Africa plate motions, as described here, resulted in changes in relative motion between the two Americas whose effects are clearly seen in the tectonic development along the northern and southern margin of the Caribbean area. Since the Caribbean plate does not appear to have moved substantially relative to the mantle during the Neogene, there are no major tectonic processes which can be attributed to the eastward 'escape' of the Caribbean plate during this time (e.g. Mann, 1997). In particular for the time since chron 6 (19 Ma), for which Caribbean–North America relative motion is better constrained than for earlier times, we find that the Caribbean plate was virtually fixed relative to the mantle.

This observation suggests that accelerated convergence post-chron 6c (23.8 Ma) at the Oligocene–Miocene boundary reduced the space within the eastward 'escaping' arc could operate such that Caribbean plate motion relative to the mantle ceased. It follows that most deformation at the northern and southern Caribbean plate boundaries in the Miocene and younger was entirely governed by changes in absolute plate motion of the North American and South American plates, and the resulting motion relative to the Caribbean plate. While strike-slip along the northern and southern Caribbean margins continued since the east–west component of absolute plate motion of the Americas was far larger than the north–south components, the magnitude of the latter increased, probably at the Oligocene–Miocene boundary, resulting in convergence between the two Americas. The rate of convergence increased from east to west, resulting in an eastward-directed 'squeeze' on the Caribbean plate which caused its breakup along the Beata Ridge, where east–west-oriented compressional stresses are absorbed (Mauffret and Leroy, Chapter 21).

Mann et al. (1995) show a model for the formation of Caribbean microplates in six stages from the Maastrichtian to present-day in a fixed South American framework. Their figures show that the Caribbean plate has moved eastward by about 800 km since the mid-Oligocene (relative to South America). Mann et al. (1995) reason that collision ceased in the Middle Eocene in central Cuba since the arc could advance no further to the north-northeast above the Bahamas Platform, and that this event rotated Caribbean plate motion clockwise in a more easterly direction. They favor the 'tectonic escape' mechanism proposed by Burke and Sengör (1986), which results in the motion of a colliding plate towards the remaining 'free face', e.g. an island arc. In case of the Caribbean in Middle Eocene times, the remaining free face would have been towards the east, i.e. the Lesser Antilles Arc. This argument is

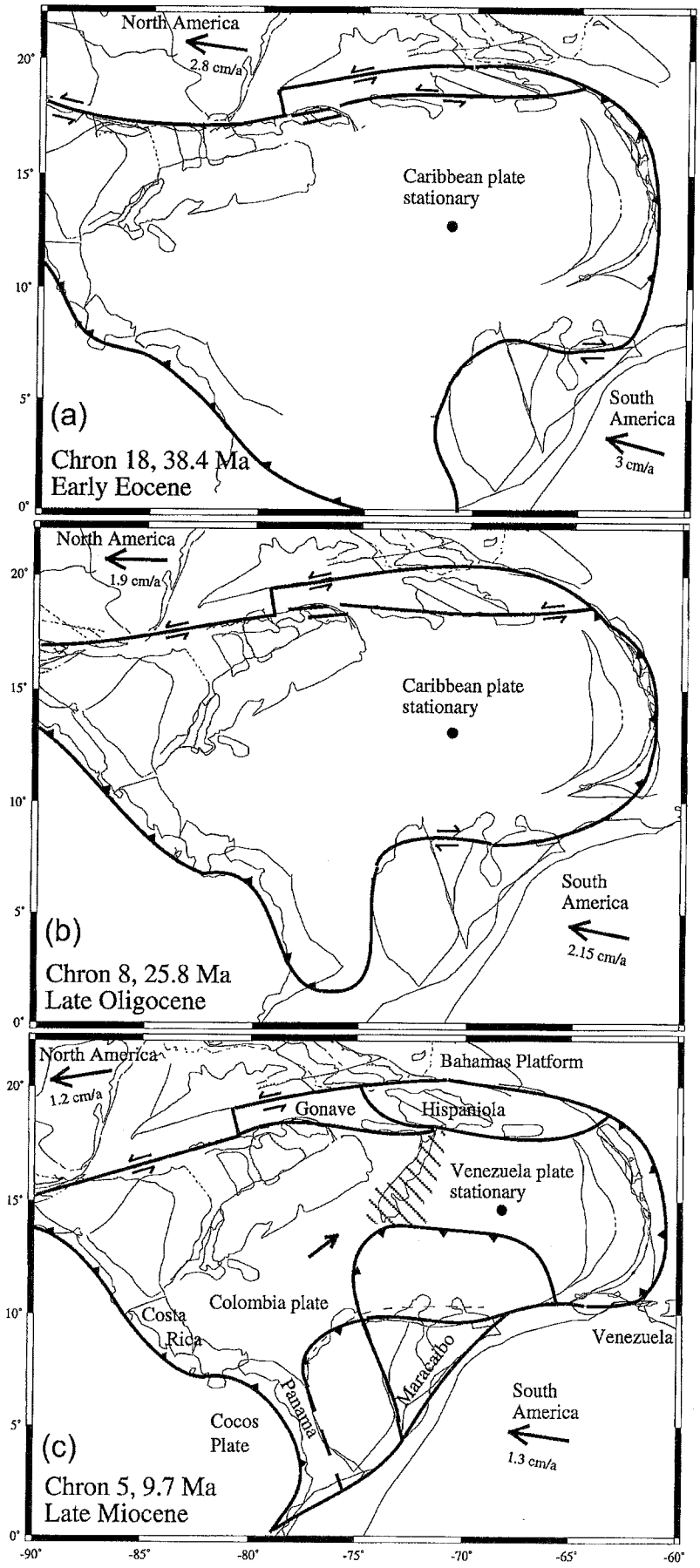
North America
2.8 cm/a
Caribbean plate
stationary
South
America
3 cm/a
(a)
Chron 18, 38.4 Ma
Early Eocene
North America
1.9 cm/a
Caribbean plate
stationary
South
America
2.15 cm/a
(b)
Chron 8, 25.8 Ma
Late Oligocene
North America
1.2 cm/a
Bahamas Platform
Gonave
Hispaniola
Venezuela plate
stationary
Colombia plate
Costa
Rica
Panama
Cocos
Plate
Maracaibo
Venezuela
South
America
1.3 cm/a
(c)
Chron 5, 9.7 Ma
Late Miocene
20°
15°
10°
5°
0°
-90°
-85°
-80°
-75°
-70°
-65°
-60°

plausible. However, if we put Caribbean plate reconstructions in the Atlantic–Indian hotspot framework (Fig. 13), it appears that the eastward motion of the Caribbean plate had ceased at Middle Eocene times.

It follows that the apparent continuing apparent 'escape' of an arc system as described by Royden (1993), e.g. for the Scotia Arc between South America and the Antarctic plate, may not necessarily involve the absolute motion of a small plate (e.g. the Scotia Sea plate) relative to the mantle. A retreating subduction boundary may be initiated by the change in polarity of a subduction system, as in the case of the proto-Caribbean, but the Caribbean plate never reached the 'open ocean' as in the case of the Scotia Sea (Royden, 1993), since its eastward migration was inhibited by boundary forces to the north and south, due to progressive convergence between the two Americas. As a result, Caribbean absolute plate motion stopped. Subsequently, all relative motion observed between the Americas and the Caribbean plate and associated tectonic elements has been caused by the absolute plate motion of North America and South America relative to a stationary Caribbean plate.

CONCLUSIONS

New gravity anomaly data from satellite altimetry and new magnetic data allow us to construct a modified plate model for plate motions between the two Americas, and calculate its uncertainties. For the North–South America plate boundary area east of the Lesser Antilles Arc our results are in good agreement with the observed strong plate deformation of the oceanic crust at the Barracuda and Tiburon ridges. Müller and Smith (1993) inverted Bouguer anomalies for crustal layer structure, and found that the Moho is uplifted 2–4 km over short wavelengths (~70 km) at the Barracuda and Tiburon ridges, implying large anelastic strains and an unstable density distribution. Together with the plate model presented here, these results indicate that much of the unusually shallow Moho topography and crustal uplift of the Tiburon Rise is a result of North America–South America convergence after chron 6 (19.0 Ma). This model is in contrast with Dolan et al.'s (1989, 1990) suggestion that the present topography of the Tiburon Rise has existed since the Late Cretaceous.

Our results suggest that slow sinistral transtension/strike-slip between the two Americas lasted from chron 34 (83 Ma) until chron 25 (55.9 Ma), followed by roughly northeast–southwest-oriented convergence until chron 18 (38.4 Ma). This first convergent phase correlates with a Paleocene–Early Eocene calc-alkaline magmatic stage in the Greater Antilles, which is thought to be related to southward subduction of proto-Caribbean crust during this time. Relatively slow transpression until chron 8 is followed by a drastic increase in convergence velocity. Subsequent to chron 8 (25.8 Ma), probably at the Oligocene–Miocene boundary, fast convergence resulted in 92 ± 22 km convergence from chron 8 to 6, 127 ± 25 km from chron 6 to 5, and 72 ± 17 km from chron 5 to the present measured at 11°N, 85°W, near the North Panama Deformed Belt. The Neogene convergence measured at the eastern Muertos Trough, at 17.5°N, 65°W, is 41 ± 18 km from chron 8 to 6, 58 ± 25 km from chron 6 to 5, and 22 ± 17 km from chron 5 to present day. The modeled conver-

Fig. 13. Plate reconstructions of the Caribbean area in an Atlantic–Indian mantle reference system for chrons 18 (38.4 Ma), 8 (25.8 Ma), and 5 (9.7 Ma). See Fig. 2 for labels of tectonic elements. Bold arrows show North American and South American plate motion relative to the mantle for the time intervals from 38.4 to 25.8 Ma (a), 25.8 to 9.7 Ma (b), and 9.7 Ma to present day (c). The eastward escape of the Caribbean plate had ceased when the opening of the Cayman Trough started (a). This time corresponds to the collision in central Cuba which prevented a further advance of the Caribbean plate to the north-northeast above the Bahamas Platform. Only if the Cayman Trough would have opened later and spread considerably faster than interpreted by Rosencrantz et al. (1988), and/or if contemporaneous strike-slip between Jamaica and the Caribbean plate was considerably faster than suggested by Burke et al. (1980), would the Caribbean plate have maintained any eastward-directed motion relative to the mantle after the Middle Eocene. (b, c) Relatively slow convergence between the Americas from chron 18 (38.4 Ma) to chron 8 (25.8 Ma) was followed by rapid convergence after chron 8, probably starting at the Oligocene–Miocene boundary, averaging 9.6 mm/year until chron 5 (9.7 Ma), slowing down to 5.2 mm/year after chron 5. Accelerated convergence was caused by a counterclockwise change in the absolute plate motion direction of North America. As a result, the total area available for the western Caribbean plate at 85°W was reduced by at least ~230 km in north–south direction in the last 25 m.y. We suggest that about half of the north–south extent (500 km) of the Maracaibo slab (subducted Caribbean oceanic plateau crust) under the South American continent (van der Hilst and Mann, 1994) may have resulted from post-Oligocene South America–Caribbean convergence. At least since chron 18 (38.4 Ma) Cocos plate–Caribbean interactions have not resulted in any substantial motion of the Caribbean plate relative to the mantle. Continuing oblique collision along the passive margin of eastern Venezuela (Algar and Pindell, 1993) must be attributed to the west-northwestward motion of South America relative to the mantle and relative to a stationary Venezuelan plate, rather than to continuing eastward movement of the Caribbean plate. Equivalently, the Miocene and younger transpression observed in Hispaniola (Heubeck and Mann, 1991) due to collision of arc rocks with the Bahamas Platform is the result of continuing westward motion of the North American plate (and the Bahamas Platform) relative to a stationary Venezuelan plate in a mantle reference frame, rather than a continuing eastward 'escape' of the Caribbean plate. The Gonave microplate has been transferred from the Venezuelan plate to North America in the Pliocene (Mann et al., 1995), leaving the rest of the Venezuelan plate behind.

gence may correspond to the Early Miocene onset of underthrusting of the Caribbean oceanic crust below the South American borderland in the Colombian and Venezuelan basins, the onset of subduction in the Muertos Trough, and folding and thrust faulting at the Beata Ridge and the Bahamas, and the breakup of the main part of the Caribbean plate into the Venezuelan and Colombian plates, separated by the Beata Ridge acting as a convergent plate boundary (Mauffret and Leroy, Chapter 21). The east–west shortening between the latter two plates may reflect the differential convergence between the two Americas, increasing from east to west.

The main differences with Pindell et al.'s (1988) model are the following.

(1) Pindell et al.'s (1988) model implies relatively constant convergence between the Americas of rates of about 5 mm/year or less since chron 21, with the exception of faster convergence between chron 6 and 5. Our model results in substantial variations in convergence rates from chron 25, as documented in Fig. 10 and Table 10. In particular, we resolve an initial phase of fast convergence between chron 8 (25.8 ma) and chron 6 (19.0 Ma) of nearly 10 mm/year, compared with less than 4 mm/year from chrons 18 to 8 measured at 85°W. We suggest that most of this convergence occurred after chron 6c (23.8 Ma), which corresponds to the Oligocene–Miocene boundary, a plate reorganization in the South Pacific (Cande et al., 1995), and the formation of the present-day deformed belts north and south of the Caribbean area. Without identifying magnetic anomaly 8, two stages of slow (chrons 13–8) and fast (chrons 8–6) convergence are averaged.

(2) We have computed uncertainties for our North America–South American plate flow lines. Uncertainty ellipses for rotated data points are especially helpful to evaluate whether or not we can resolve relatively slow phases of relative motion.

(3) We have put Caribbean plate reconstructions into the Atlantic–Indian hotspot reference system from Müller et al. (1993). This allows us to evaluate causes and effects of relative plate motions in the Caribbean area.

Stéphan et al. (1986) put forward the hypothesis that both the northern and the southern Caribbean deformed belts are the result of the bending of the Caribbean continental frame related to east–west shortening. East–west shortening appears to have a variety of different causes. In the Panama area, east–west shortening is related to Nazca–South America convergence in that direction and collision of an east–west-oriented arc with a north–south-oriented margin (Mann and Corrigan, 1990; Wadge and Burke, 1983). In Hispaniola, northeast–southwest shortening is related to the interaction of the westward-moving North American plate relative to a stationary Caribbean plate as shown before.

Our plate model shows well resolved north–south convergence between the Americas during the Neogene, and we argue that this plate convergence is likely the main cause for the formation of those deformed belts which cannot be attributed to east–west convergence as described above. We also suggest that the fast Neogene plate convergence between North and South America contributed to the Late Miocene onset of the collision of the Costa Rica–Panama Arc with the western Cordillera of South America (Wadge and Burke, 1983; Eva et al., 1989; Mann et al., 1990; Mann and Corrigan, 1990). One of the main tectonic events affecting the Caribbean plate in the Neogene has been its breakup into the Venezuelan and Colombian plates (see Mauffret and Leroy, Chapter 21). The breakup may have been caused the observed east–west gradient in convergence between the Americas, the subduction of the buoyant Cocos plate under the Caribbean plate (Mauffret and Leroy, Chapter 21), or the north-northeastward motion of the Maracaibo block, which in turn may be related to differential North–South America convergence.

By combining Atlantic–Indian hotspots as a reference frame with revised North America–African and South America–African relative plate motions, and with a revised plate model for the Caribbean area we are able to show the following.

(1) The eastward escape of the Caribbean plate appears to have ceased when the opening of the Cayman Trough started. This time corresponds to the collision in central Cuba which prevented a further advance of the Caribbean plate to the north-northeast above the Bahamas Platform. Only if the Cayman Trough would have opened later and spread considerably faster than interpreted by Rosencrantz et al. (1988), and/or if contemporaneous strike-slip between Jamaica and the Caribbean plate was considerably faster than suggested by Burke et al. (1980) would the Caribbean plate have maintained any eastward-directed motion relative to the mantle after the Middle Eocene. If we rely only on the interpreted post-chron-6 (19 Ma) spreading history of the Cayman Trough by Rosencrantz et al. (1988), which is better constrained than its previous opening, then the Caribbean plate is still found to have been without any substantial motion relative to the mantle subsequent to chron 6 within the errors of absolute plate motion models.

(2) It is not the case that North America–South America plate motions had only minor effects on the development of the Caribbean region after the Campanian, as suggested by Pindell et al. (1988). After the breakup of the Caribbean plate into the Venezuelan and Colombian plates, the eastward driving force

of the latter plate may have still been derived from interactions with the Cocos plate. However, even if this is so, our model suggests that post-chron-8 (25.8 Ma) differential motion between the Americas has resulted in a total of 291 ± 64 km in convergence at 85°W near the North Panama Deformed Belt. In other words, the total area available for the Colombian plate at 85°W was reduced by at least ~230 km in north–south direction in the last 25 m.y. Surely this reduction in space had a profound influence on the Colombian plate margin, and has contributed to convergence along the North Panama Deformed Belt. van der Hilst and Mann (1994) show that the subducted Maracaibo slab underlying northwestern South America extends up to 500 km from the Caribbean–South America boundary to the south. The Maracaibo slab corresponds to subducted Caribbean oceanic plateau crust. Our results suggest that about half of the north–south extent of the Maracaibo slab under the South American continent may have resulted from Miocene and later South America–Caribbean convergence, if most of the North America–South America convergence was taken up at this boundary.

(3) The Caribbean plate has been trapped between two larger plates, and has been subject to edge-driven plate tectonic interactions since then. It follows that the main control on North America–Caribbean and South America–Caribbean plate interactions has not originated from Cocos plate–Caribbean interactions, as these interactions have not resulted in any substantial motion of the Caribbean plate relative to the mantle. Continuing oblique collision along the passive margin of eastern Venezuela as reported by Algar and Pindell (1993) must be attributed to the west-northwestward motion of South America relative to the mantle and relative to a stationary Venezuelan plate, rather than to continuing eastward movement of the Caribbean plate. Equivalently, the Miocene and younger transpression observed in Hispaniola (Heubeck and Mann, 1991) due to collision of arc rocks with the Bahamas Platform is the result of continuing westward motion of the North American plate (and the Bahamas Platform) relative to an approximately stationary Venezuelan plate in a mantle reference frame, rather than a continuing eastward 'escape' of the Caribbean plate. By the same token, the Gonave microplate, which has been detached from the Caribbean microplate in the Pliocene and accreted to North America has not been 'left behind' (Mann et al., 1995), but has rather been transferred from a stationary Venezuelan plate to North America, leaving the rest of the Venezuelan plate behind.

(4) The Tertiary tectonic history of the Caribbean plate can be described by 'tectonic escape' up to the Middle Eocene. Subsequently the Caribbean plate came to a halt in the Atlantic–Indian mantle reference system due to a progressive reduction in space between the two Americas for the arc to move eastward and due to its collision with the Bahamas Platform. We show that the most severe reduction in space started at the Oligocene–Miocene boundary, resulting in the gradual formation of many of today's tectonic elements and sedimentary basins in the Caribbean area.

ACKNOWLEDGEMENTS

The contents of this paper have been clarified substantially by Jim Pindell's comprehensive review of an early draft. Given that we are no experts on Caribbean geology, our discussion and the interpretation of our results has benefited from many discussions with Eric Calais and Alain Mauffret, as well as from thorough reviews by Jan Golonka, Mark Gordon, and Ian Norton. We thank Paul Mann for his encouragement to make a contribution to this volume. JYR acknowledges support from the Centre Nationale de la Recherche Scientifique (CNRS) that enabled his visit at the University of Sydney, and from the Plan Nationale de Teledetection Spatiale. UMR 6526 Géosciences Azur contribution 139, Geological Survey of Canada contribution 1997027.

REFERENCES

Adamek, S., Tajima, F. and Wiens, D.A., 1987. Seismic rupture associated with subduction of the Cocos Ridge. Tectonics, 6: 757–774.

Algar, S.T. and Pindell, J.L., 1993. Structure and deformation history of the Northern Range of Trinidad and adjacent areas. Tectonics, 12: 814–829.

Biju-Duval, B., Mascle, A., Rosales, H. and Young, G., 1984. Episutural Oligo-Miocene basins along the North Venezuelan margin. In: J.S. Watkins and C.L. (Editors), Drake Studies in Continental Margin Geology. Am. Assoc. Pet. Geol. Mem., 34: 347–358.

Bralower, T.J., Hutson, F., Mann, P., Iturralde-Vinent, M., Renne, P. and Sliter, W.V., 1993. Tectonics of oblique arc–continent collision in western Cuba, 1. Stratigraphic constraints. Eos, Trans. Am. Geophys. Union, 74: 546.

Burke, K. and Sengör, C., 1986. Tectonic escape in the evolution of the continental crust. In: Barazangi, M. and Brown, L. (Eds.), Reflection Seismology: The Continental Crust. Geodyn. Ser. 14, Am. Geophys. Un., Washington, D.C., pp. 41–53.

Burke, K., Fox, P. and Sengör, A.M.C., 1978. Buoyant ocean floor and the evolution of the Caribbean. J. Geophys. Res., 83: 3949–3954.

Burke, K., Grippi, J. and Sengör, A.M.C., 1980. Neogene structures in Jamaica and the tectonic style of the northern Caribbean plate boundary zone. J. Geol., 88: 375–386.

Byrne, D.B., Suarez, G. and McCann, W.R., 1985. Muertos Trench subduction — microplate tectonics in the northern Caribbean? Nature, 317: 420–421.

Calais, E., Stéphan, J.-F., Beck, Ch., Carfantan, J.-Ch., Tardy, M.,

Thery, J.-M., Olivet, J.-L., Bouysse, Ph., Mercier de Lépinay, B., Tournon, J., Vila, J.-M., Mauffret, A., Blanchet, R., Bourgois, J. and Dercourt, J., 1989. Évolution paléogéographique et structurale du domaine caraïbe du Lias à l'Actuel: 14 étapes pour 3 grandes périodes. C. R. Acad. Sci. Paris, 309: 1437–1444.

Calais, E., Béthoux, N. and Mercier de Lépinay, B., 1992. From transcurrent faulting to frontal subduction: a seismotectonic study of the Northern Caribbean plate boundary from Cuba to Puerto Rico. Tectonics, 11: 114–123.

Cande, S.C. and Kent, D.V., 1995. Revised calibration of the geomagnetic time scale for the late Cretaceous and Cenozoic. J. Geophys. Res., 100: 6093–6098.

Cande, S.C., LaBrecque, J.L. and Haxby, W.F., 1988. Plate kinematics of the South Atlantic: chron 34 to present. J. Geophys. Res., 93: 13,479–13,492.

Cande, S.C., Raymond, C.A., Haxby, W.F. and Haxby, W.F., 1995. Geophysics of the Pitman Fracture Zone and Pacific–Antarctic plate motions during the Cenozoic. Science, 270: 947–953.

Case, J.E., Holcombe, T.L. and Martin, R.G., 1984. Map of geological provinces in the Caribbean region. In: W.E. Bonini, R.B. Hargraves and R. Shagam (Editors), The Caribbean–South America Plate Boundary and Regional Tectonics. Geol. Soc. Am. Mem., 162: 1–30.

Chang, T., 1987. On the statistical properties of estimated rotations. J. Geophys. Res., 92: 6319–6329.

Chang, T., 1988. On reconstructing tectonic plate motion from ship track crossing. J. Am. Stat. Assoc., 83: 1178–1183.

Chang, T., Stock, J. and Molnar, P., 1990. The rotation group in plate tectonics and the representation of uncertainties of plate reconstructions. Geophys. J. Int., 101: 649–661.

Collette, B.J., Slootweg, A.P., Verhoef, J. and Roest, W.R., 1984. Geophysical investigations of the floor of the Atlantic Ocean between 10° and 38°N (Kroonvlag-project). Proc. Kon. Ned. Akad. Wet., Ser. B, 87: 1–76.

DeMets, C., Gordon, R.G., Argus, D.F. and Stein, S., 1990. Current plate motions. Geophys. J. Int., 101: 425–478.

Dixon, T.H. and Mao, A., 1997. A GPS estimate of relative motion between North and South America. Geophys. Res. Lett., 24: 535–538.

Dolan, J.F., Beck, Ch. and Ogawa, Y., 1989. Upslope deposition of extremely distal turbidites: an example from the Tiburon Rise, west-central Atlantic. Geology, 17: 990–994.

Dolan, J.F., Beck, Ch., Ogawa, Y. and Klaus, A., 1990. Eocene–Oligocene sedimentation in the Tiburon Rise/ODP Leg 110 area: an example of significant upslope flow of distal turbidity currents. Proc. ODP, Sci. Results, 110: 47–62.

Ego, F., Sebrier, M. and Yepes, H., 1995. Is the Cauca–Patia and Romeral fault system left or right lateral? Geophys. Res. Lett., 22: 33–36.

Elsasser, W.M., 1971. Sea-floor spreading as thermal convection. J. Geophys. Res., 76: 1101–1112.

Engebretson, D., 1982. Model presentation for displacements between western North America, eastern Eurasia, and adjacent oceanic plates for the past 180 million years. In: Circum-Pacific energy and mineral resources conference, AAPG Bull. 66: 966,

Engebretson, D.C., Cox, A. and Gordon, R.G., 1985. Relative motions between oceanic and continental plates in the Pacific Basin. Geol. Soc. Am. Spec. Pap., 206, 59 pp.

England, P. and Wortel, R., 1980. Some consequences of the subduction of young slab. Earth Planet. Sci. Lett., 47: 403–415.

Eva, A.N., Burke, K., Mann, P. and Wadge, G., 1989. Four-phase tectonostratigraphic development of the southern Caribbean. Mar. Pet. Geol., 6: 9–21.

Gripp, A.E. and Gordon, R.G., 1990. Current plate velocities relative to the hotspots incorporating the NUVEL-1 global plate motion model. Geophys. Res. Lett., 17: 1109–1112.

Gradstein, F.M., Agterberg, F.P., Ogg, J.G., Hardenbol, J., van Veen, P., Thierry, J. and Huang, Z., 1994. A Mesozoic time scale. J. Geophys. Res., 99: 24,051– 24,074.

Harrison, C.G.A. and Lindh, T., 1982. A polar wandering curve for North America during the Mesozoic and Cenozoic. J. Geophys. Res., 87: 1903–1920.

Hellinger, S.J., 1981. The uncertainties in finite rotations in plate tectonics. J. Geophys. Res., 86: 9312–9318.

Heubeck, C. and Mann, P., 1991. Geologic evaluation of plate kinematic models for the North American–Caribbean plate boundary zone. Tectonophysics, 191: 1–26.

Heubeck, C., Mann, P., Dolan, J. and Monechi, S., 1991. Diachronous uplift and recycling of sedimentary basins during Cenozoic tectonic transpression, northeastern Caribbean plate margin. Sediment. Geol., 70: 1–32.

Kent, D.V. and Gradstein, F.M., 1986. A Jurassic to Recent chronology. In: P.R. Vogt and B.E. Tucholke (Editors), The Western North Atlantic Region. The Geology of North America, Vol. M, Geological Society of America, Boulder, CO, pp. 45–50.

Klitgord, K.D. and Schouten, H., 1986. Plate kinematics of the central North Atlantic. In: P.R. Vogt and B.E. Tucholke (Editors), The Western North Atlantic Region. The Geology of North America, Vol. M, Geological Society of America, Boulder, CO, pp. 351–404.

Ladd, J.W., 1976. Relative motion of South America with respect to North America and Caribbean tectonics. Geol. Soc. Am. Bull., 87: 969–976.

Ladd, J.W., Truchan, M., Talwani, M., Stoffa, P.L., Buhl, P., Houtz, R., Mauffret, A. and Westbrook, G., 1984. In: W.E. Bonini, R.B. Hargraves and R. Shagam (Editors), The Caribbean–South America Plate Boundary and Regional Tectonics. Geol. Soc. Am. Mem., 162: 153–160.

Ladd, J.W., Holcombe, T.L., Westbrook, G.K. and Edgar, N.T., 1990. Caribbean marine geology; active margins of the plate boundary. In: G. Dengo and J.E. Case (Editors), The Caribbean Region. The Geology of North America, Geological Society of America, Vol. H, Boulder, CO, pp. 261–290.

Mann, P., 1997. Model for the formation of large, transtensional basins in zones of tectonic escape. Geology, 25: 211–214.

Mann, P. and Burke, K., 1984. Neotectonics of the Caribbean. Rev. Geophys. Space Phys., 22: 309–362.

Mann, P. and Corrigan, J., 1990. Model for late Neogene deformation in Panama. Geology, 18: 558–562.

Mann, P., Schubert, C. and Burke, K., 1990. Review of Caribbean neotectonics. In: G. Dengo and J.E. Case (Editors), The Caribbean Region. The Geology of North America, Vol. H, Geological Society of America, Boulder, CO, pp. 307–338.

Mann, P., Taylor, F., Edwards, L. and Ku, T., 1995. Actively evolving microplate formation by oblique collision and sideways motion along strike-slip faults: an example from the northeastern Caribbean plate margin. Tectonophysics, 246: 1–69.

Maschenkov, S. and Pogrebitsky, Y., 1992. Preliminary results of Canary–Bahamas Project. Eos, Trans. Am. Geophys. Union, 73: 393–397.

Mascle, J., Blarez, E. and Marinho, M., 1988. The shallow structures of the Guinea and Ivory Coast–Ghana transform margins: their bearing on the Equatorial Atlantic Mesozoic evolution. Tectonophysics, 155: 193–210.

McKenzie, D., 1972. Active tectonics of the Mediterranean region. Geophys. J. R. Astron. Soc., 30: 109–185.

Meijer, P.T., 1992. The dynamics of motion of the South America plate. J. Geophys. Res., 97: 11,915–11,931.

Molnar, P. and Stock, J., 1987. Relative motions of hotspots in

the Pacific, Atlantic and Indian Oceans since late Cretaceous time. Nature, 327: 587–591.

Müller, R.D. and Roest, W.R., 1992. Fracture zones in the North Atlantic from combined Geosat and Seasat data. J. Geophys. Res., 97: 3337–3350.

Müller, R.D. and Smith, W.H.F., 1993. Deformation of the oceanic crust between the North America and South America plates. J. Geophys. Res., 93: 8275–8292.

Müller, R.D., Sandwell, D.T., Tucholke, B.E., Sclater, J.G. and Shaw, P.R., 1991. Depth to basement and geoid expression of the Kane Fracture Zone: a comparison. Mar. Geophys. Res., 13: 105–129.

Müller, R.D., Royer, J.-Y. and Lawver, L.A., 1993. Revised plate motions relative to the hotspots from combined Atlantic and Indian Ocean hotspot tracks. Geology, 21: 275–278.

Müller, R.D., Roest, W.R., Royer, J.-Y., Gahagan, L.M. and Sclater, J.G., 1997. Digital isochrons of the world's ocean floor. J. Geophys. Res., 102: 3211–3214.

Perfit, M.R. and Heezen, B.C., 1978. The geology and evolution of the Cayman Trench. Geol. Soc. Am. Bull., 89: 1155–1174.

Pindell, J.L. and Barrett, S.F., 1990. Geological evolution of the Caribbean region; a plate tectonic perspective. In: G. Dengo and J.E. Case (Editors), The Caribbean Region. The Geology of North America, Geological Society of America, Vol. H, Boulder, CO, pp. 405–432.

Pindell, J.L. and Dewey, J.F., 1982. Permo-Triassic reconstruction of western Pangea and the evolution of the Gulf of Mexico/Caribbean region. Tectonics, 1: 179–212.

Pindell, J.L., Cande, S.C., Pitman, W.C., III, Rowley, D.B., Dewey, J.F., LaBrecque, J. and Haxby, W., 1988. A plate-kinematic framework for models of Caribbean evolution. Tectonophysics, 155: 121–138.

Plafker, G. and Ward, S.N., 1992. Thrust faulting and tectonic uplift along the April 1922, 1991 Costa Rica earthquake. Tectonics, 11: 709–718.

Roest, W.R. and Collette, B.J., 1986. The Fifteen Twenty Fracture Zone and the North American–South America plate boundary. J. Geol. Soc. London, 143: 833–843.

Rona, P.A., 1980. The central North Atlantic Ocean Basin and continental margins: geology, geophysics, geochemistry, and resources, including the trans-Atlantic geotraverse (TAG). National Oceanic and Atmospheric Administration/NOAA Atlas 3.

Rosencrantz, E., 1990. Structure and tectonics of the Yucatan basin, Caribbean Sea, as determined from seismic reflection studies. Tectonics, 9: 1037–1059.

Rosencrantz, E. and Mann, P., 1991. SeaMARC II mapping of transform faults in the Cayman trough, Caribbean Sea. Geology, 19: 2141–2157.

Rosencrantz, E., Ross, M.I. and Sclater, J.G., 1988. Age and spreading history of the Cayman trough as determined from depth, heat flow, and magnetic anomalies. J. Geophys. Res., 93: 2141–2157.

Rosenfeld, J.H., 1990. Sedimentary rocks of the Santa Cruz ophiolite — a proto-Caribbean history. Trans. 12th Caribbean Geol. Conf., U.S. Virgin Islands, pp. 513–519.

Ross, M.I. and Scotese, C.R., 1988. A hierarchical tectonic model of the Gulf of Mexico and Caribbean region. Tectonophysics, 155: 139–168.

Royden, L.H., 1993. Evolution of retreating subduction boundaries formed during continental collision. Tectonics, 12: 629–638.

Royer, J.-Y. and Chang, T., 1991. Evidence for relative motions between the Indian and Australian plates during the last 20 Myr from plate tectonic reconstructions: implications for the deformation of the Indo-Australian plate. J. Geophys. Res., 96: 11,779–11,802.

Royer, J.-Y., Gordon, R.G., DeMets, C. and Vogt, P.R., 1997. New limits on the motion between India and Australia since chron 5 (11 Ma) and implications for lithospheric deformation in the equatorial Indian Ocean. Geophys. J. Int., 129: 41–74.

Sandwell, D.T. and Smith, W.H.F., 1997. Marine gravity anomaly from Geosat and ERS-1 satellite altimetry. J. Geophys. Res., 102: 10,039–10,054.

Shaw, P.R. and Cande, S.C., 1990. High-resolution inversion for South Atlantic plate kinematics using joint altimeter and magnetic anomaly data. J. Geophys. Res., 95: 2625–2644.

Stéphan, J.F., Blanchet, R. and Mercier de Lépinay, B., 1986. Northern and southern Caribbean festoons (Panama, Colombian–Venezuela and Hispaniola–Puerto Rico), interpreted as pseudosubdivisions induced by the east–west shortening of the peri-Caribbean continental frame. In: Wezel-Forese, C. (Ed.), The Origin of Arcs. Developments in Geotectonics, vol. 21, Elsevier, Amsterdam, pp. 401–422.

Stéphan, J.F., Mercier De Lépinay, B., Calais, E., Tardy, M., Beck, Ch., Carfantan, J.-Ch., Olivet, J.-L., Vila, J.-M., Bouysse, Ph., Mauffret, A., Bourgois, J., Thery, J.-M., Tournon, J., Blanchet, R. and Dercourt, J., 1990. Paleogeodynamic maps of the Caribbean: 14 steps from Lias to Present. Bull. Soc. Géol. Fr., 8: 915–919.

Stock, J. and Molnar, P., 1983. Some geometrical aspects of uncertainties in combined plate reconstructions. Geology, 11: 697–701.

Sykes, L.R., McCann, W.R. and Kafka, A.L., 1982. Motion of Caribbean plate during last 7 million years and implications for earlier Cenozoic movements. J. Geophys. Res., 87: 10,656–10,676.

Tucholke, B.E. and Schouten, H., 1988. Kane fracture zone. Mar. Geophys. Res., 10: 1–39.

Van der Hilst, R. and Mann, P., 1994. Tectonic implications of tomographic images of subducted lithosphere beneath northwestern South America. Geology, 22: 451–454.

Wadge, G. and Burke, K., 1983. Neogene Caribbean plate rotation and associated tectonic evolution. Tectonics, 2: 633–643.